JACS
JOURNAL OF THE AMERICAN CHEMICAL SOCIETY
Article
Cite This: J. Am. Chem. Soc. 2018, 140, 8463−8478
pubs.acs.org/JACS

Three-Fold Intramolecular Ring Closing Alkene Metatheses of Square Planar Complexes with *cis* Phosphorus Donor Ligands $P(X(CH_2)_mCH{=}CH_2)_3$ (X = −, *m* = 5−10; X = O, *m* = 3−5): Syntheses, Structures, and Thermal Properties of Macrocyclic Dibridgehead Diphosphorus Complexes

Hemant Joshi,[†,§] Sugam Kharel,[†,§] Andreas Ehnbom,[†] Katrin Skopek,[‡] Gisela D. Hess,[‡] Tobias Fiedler,[†] Frank Hampel,[‡] Nattamai Bhuvanesh,[†] and John A. Gladysz*[,†,‡]

[†]Department of Chemistry, Texas A&M University, PO Box 30012, College Station, Texas 77842-3012, United States
[‡]Institut für Organische Chemie and Interdisciplinary Center for Molecular Materials, Friedrich-Alexander-Universität Erlangen-Nürnberg, Henkestraße 42, 91054 Erlangen, Germany

Supporting Information

ABSTRACT: Reactions of *cis*-$PtCl_2(P((CH_2)_mCH{=}CH_2)_3)_2$ and Grubbs' first generation catalyst and then hydrogenations afford *cis*-$PtCl_2(P((CH_2)_n)_3P)$ (*cis*-**2**; *n* = 2*m* + 2 = 12 (**b**), 14 (**c**), 16 (**d**), 18 (**e**), 20 (**f**), 22 (**g**); 6−40%), derived from 3-fold *interligand* metatheses. The phosphite complexes *cis*-$PtCl_2(P(O(CH_2)_{m*}CH{=}CH_2)_3)_2$ are similarly converted to *cis*-$PtCl_2(P(O(CH_2)_{n*}O)_3P)$ (*cis*-**5**; *n** = 8 (**a**), 10 (**b**), 12 (**c**), 10−20%). The substitution products *cis*-$PtPh_2(P((CH_2)_n)_3P)$ (*cis*-**6c**,**d**) and *cis*-$PtI_2(P(O(CH_2)_{10}O)_3P)$ are prepared using Ph_2Zn and NaI, respectively. Crystal structures of *cis*-**2c**,**d**,**f**, *cis*-**5a**,**b**, and *cis*-**6c** show one methylene bridge that roughly lies in the platinum coordination plane and two that are perpendicular. The thermal behavior of the complexes is examined. When the bridges are sufficiently long, they rapidly exchange via an unusual "triple jump rope" motion over the PtX_2 moieties. NMR data establish $\Delta H^{\ddagger}$, $\Delta S^{\ddagger}$, and $\Delta G^{\ddagger}_{298K}/\Delta G^{\ddagger}_{393K}$ values of 7.8 kcal/mol, −27.9 eu, and 16.1/18.8 kcal/mol for *cis*-**2d**, and a $\Delta G^{\ddagger}_{393K}$ of ≥19.6 kcal/mol for the shorter bridged *cis*-**2c**. While *cis*-**2c**,**g** gradually convert to *trans*-**2c**,**g** at 150−185 °C in haloarenes, *trans*-**2c**,**g** give little reaction under analogous conditions, establishing the stability order *trans* > *cis*. Similar metathesis/hydrogenation sequences with octahedral complexes containing two *cis* phosphine ligands, *fac*-$ReX(CO)_3(P((CH_2)_6CH{=}CH_2)_3)_2$ (X = Cl, Br), give *fac*-$ReX(CO)_3(P(CH_2)_{13}CH_2)((CH_2)_{14})(P(CH_2)_{13}CH_2)$ (19−50%), which are derived from a combination of *interligand* and *intraligand* metathesis. The relative stabilities of *cis*/*trans* and other types of isomers are probed by combinations of molecular dynamics and DFT calculations.

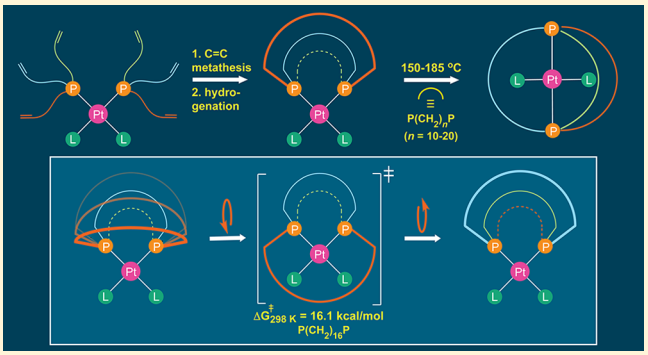

1. INTRODUCTION

Multifold ring closing alkene (C=C) metatheses can lead to a variety of fascinating molecular architectures, especially in metal coordination spheres.[1,2] Over the last 15 years, we have been especially concerned with metathesis/hydrogenation sequences of the type exemplified in Scheme 1.[3−7] These feature educts with *trans* disposed olefinic phosphine ligands of the formula $P((CH_2)_mCH{=}CH_2)_3$, such as the platinum dichloride complexes *trans*-**1c**−**e** (indices code to the number of atoms between phosphorus and the vinyl group). The major products are almost always derived from 3-fold *interligand* metatheses, which afford triply *trans* spanning dibridgehead diphosphine ligands. For *trans*-**1c**−**e**, this corresponds to *trans*-**2c**−**e**. In some cases, byproducts derived from combinations of *interligand* and *intraligand* metatheses are obtained, such as *trans*-**2′c**−**e** in Scheme 1. Such species carry primed numbers throughout this manuscript. Setaka has realized similar chemistry when the P−M−P linkages are replaced by Si−arylene−Si linkages (e.g., arylene = *p*-C_6H_4).[2d,8]

Analogous reactions of palladium complexes with shorter methylene chains have been investigated, but only oligomeric or polymeric products were detected.[4b,9] In any event, the mono-platinum complexes *trans*-**2c**−**e** represent an interesting class of molecular rotors.[10] In all cases, rotation of the $PtCl_2$ moieties about the P−Pt−P axes is rapid on the NMR time scale, even at

Received: March 14, 2018
Published: April 30, 2018

DOI: 10.1021/jacs.8b02846
J. Am. Chem. Soc. 2018, 140, 8463−8478

Scheme 1. Three-fold Ring Closing Metatheses of *trans*-1c–e: Syntheses of Gyroscope-like Complexes *trans*-2c–e[4]

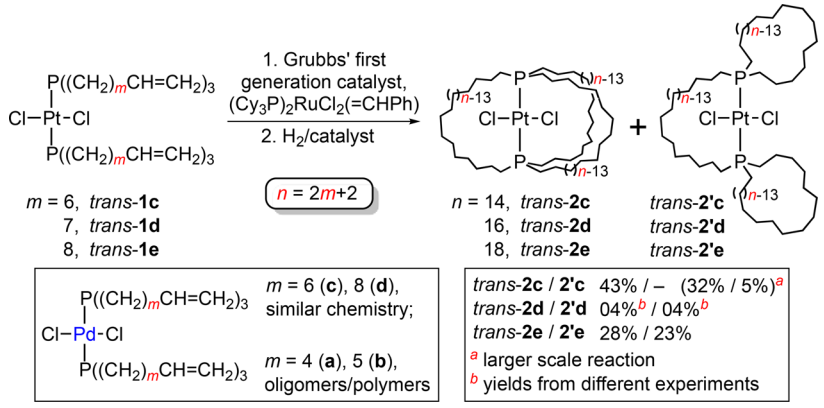

Scheme 2. Three-fold Ring Closing Metatheses of *cis*-1b–g: Syntheses of Parachute-like Complexes *cis*-2b–g

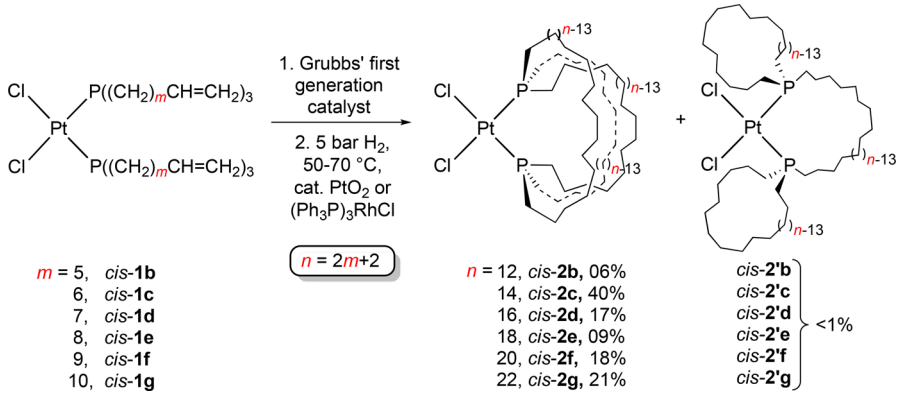

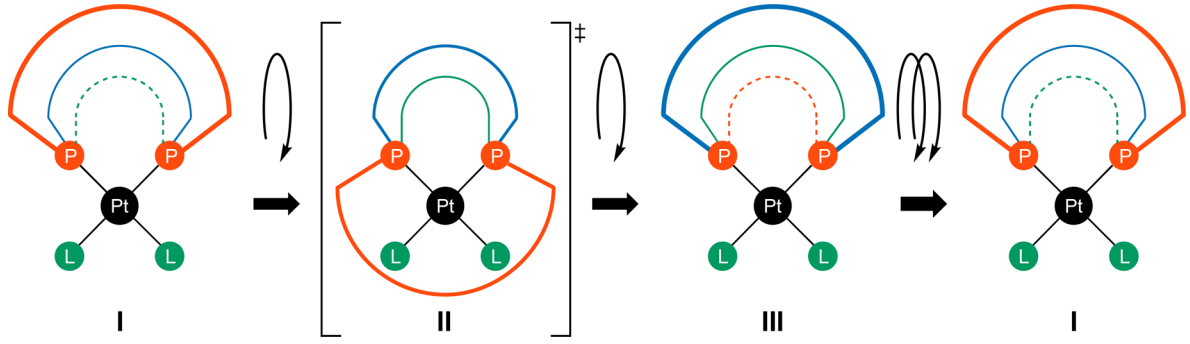

Figure 1. Possible "jump rope" dynamic processes involving the macrocycles of parachute-like complexes *cis*-**2**.

−80 °C.[4,11] Given the suggestive geometry, and the potential for closely related systems to function as molecular gyroscopes,[8,10,12,13] we refer to them as gyroscope-like.

During the course of the efforts in Scheme 1, syntheses of the isomeric educts *cis*-**1** were developed.[14] Hence, it became of interest to investigate analogous metathesis/hydrogenation sequences, as sketched in Scheme 2. In the case of 3-fold *interligand* metathesis to give *cis*-**2**, a likely spatial distribution of macrocycles suggests (when the perpendicular Pt–Cl bonds are both directed downward) a parachute (see **I** in Figure 1). Thus, we refer to *cis*-**2** as parachute-like.

Such complexes can also potentially serve as molecular rotors, although this is now in the form of coupled motion about two perpendicular Pt–P bonds. From the frame of reference of the Cl–Pt–Cl moiety, this may be viewed as a 3-fold "jump rope" process, as illustrated in Figure 1.[15] To wit, one methylene chain occupies a "central" position roughly in the platinum coordination plane and the other two flanking positions above and below the coordination plane. These undergo clockwise or counterclockwise exchange in the same sense as "jumping rope" (or a tripled rope) in forward or backward directions. Others have made "jump rope" analogies for dynamic processes involving a *single* methylene or methylene rich bridge,[15] but *cis*-**2** is perhaps the first system to invoke the rich Olympic traditions of the triple jump or triple axel.

Apart from any dynamic properties, such adducts are of interest in that they help define the geometric flexibility of the dibridgehead diphosphine ligands $P((CH_2)_n)_3P$ (**3c–e**), which can be isolated via various demetalation protocols.[4,16] Both **3c** and **3e** have been found to serve as "container molecules" capable of transporting MCl_2 moieties from one aqueous phase to another.[17] In all cases, when the "containers" **3c,e** are "loaded" (M = Pt, Pd, Ni), the resulting adducts exhibit *trans* Cl–M–Cl and P–M–P linkages (i.e., *trans*-**2c** as opposed to *cis*-**2c**), as exemplified in Scheme 3.

DOI: 10.1021/jacs.8b02846
J. Am. Chem. Soc. 2018, 140, 8463–8478

Scheme 3. Homeomorphic Isomerization of Macrocyclic Dibridgehead Diphosphines and Complexation of MCl_2 Units

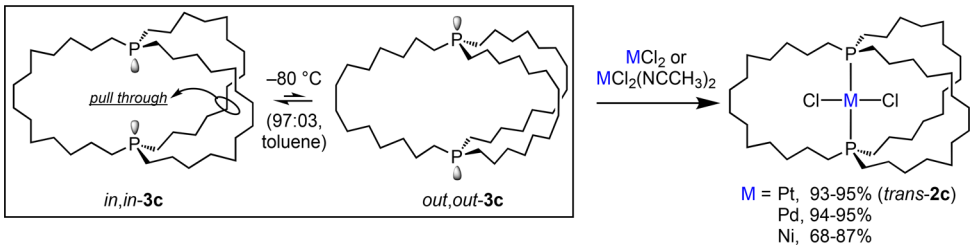

We have sought to better understand the nuances of this process, especially with respect to kinetic and thermodynamic control of geometric isomerism. The dibridgehead diphosphines are themselves capable of dynamic processes, such as "homeomorphic isomerization",[18] which exchanges *exo* directed (*out,out*) and *endo* directed (*in,in*) functionality without any intervening inversions of configuration at phosphorus (Scheme 3). However, these phenomena do not play a role in this study.

Accordingly, we set out to (1) synthesize the parachute-like complexes in Scheme 2, as well as homologues with dibridgehead diphosphite ligands or octahedral coordination geometries, (2) characterize their spectroscopic, structural, and dynamic properties, and (3) probe their stabilities vis-à-vis gyroscope-like isomers by both experimental and computational techniques. A small portion of this work has been communicated.[19]

2. RESULTS

2.1. Syntheses, Dibridgehead Diphosphine Series. The educts *cis*-$PtCl_2(P((CH_2)_mCH{=}CH_2)_3)_2$ (*cis*-**1**) were prepared from K_2PtCl_4 and the constituent olefinic phosphines in water as reported earlier (*cis*-**1b–e**; m = 5–8, 33–70%)[14] or by extending the protocol to phosphines with longer methylene chains (*cis*-**1f,g**; m = 9,10, 44–51%; Supporting Information (SI)). Minor amounts of *trans*-**1** were often noted but were easily separated chromatographically (*trans*-**1** dominates when syntheses are conducted using $PtCl_2$ and the less polar solvent benzene).[14] In accord with literature precedent for bis(phosphine) platinum(II) complexes,[20] the $^1J_{PPt}$ values of *cis*-**1b–g** were much greater than those of *trans*-**1b–g** (3511–3518 vs 2375–2382 Hz).[4]

As shown in Scheme 2, dilute CH_2Cl_2 solutions of *cis*-**1b–g** (0.00073–0.0015 M) and Grubbs' first generation catalyst (7.5–12 mol %) were refluxed. After 12–48 h, workups gave crude metathesis products. The $^{31}P\{^1H\}$ NMR spectra exhibited a multitude of signals,[21] some of which presumably reflect *cis*/*trans* C=C isomers. Hydrogenations were carried out under 1–5 bar of H_2 using PtO_2 or $(Ph_3P)_3RhCl$ as catalysts. Workups gave the target parachute-like dibridgehead diphosphine complexes *cis*-$PtCl_2(P((CH_2)_n)_3P)$ (*cis*-**2b–g**; $n = 2m + 2$) in 6–40% overall yields. The P–Pt–P moieties are part of 15- to 25-membered macrocycles. No other monoplatinum products were detected. Hence, the generally low mass balance presumably reflects the formation of oligomers.[21b] Yields were nearly the same when Grubbs' second generation catalyst was employed.

All new complexes that were not mixtures of isomers were characterized by NMR (^1H, ^{13}C, ^{31}P) and in many cases by microanalyses, mass spectrometry, and IR spectroscopy, as summarized in section 4. The structures of *cis*-**2b–g** readily followed from their spectroscopic properties. For example, the $^1J_{PPt}$ values were much greater than those of the *trans* isomers in Scheme 1 (3530–3568 vs 2389–2398 Hz). With *cis*-**2b–d**, two sets of methylene ^{13}C signals were observed, with an intensity ratio of ca. 2:1. With *cis*-**2e–g**, only a single set of methylene signals was observed. This dichotomy is rationalized below. Importantly, the isomeric structures *cis*-**2′b–g** (Scheme 2), which are derived from a combination of *interligand* and *intraligand* metatheses, would give two sets of signals for all macrocycle sizes (the less intense from the methylene chain that spans the two phosphorus atoms; the more intense from the phosphacycle methylene chains that circle back to the same phosphorus atom).

2.2. Syntheses, Dibridgehead Diphosphite Series. Bis(phosphite) dihaloplatinum complexes are usually obtained as *cis* isomers,[22] consistent with the greater π acidities of phosphite as compared to trialkylphosphine ligands. However, a few special types of *trans* isomers have been reported.[23] The latter feature much lower $^1J_{PPt}$ values (4405–4680 vs 5694–5918 Hz).[22,23] Thus, the olefinic phosphites $P(O(CH_2)_{m^*}CH{=}CH_2)_3$ (m^* = 3 (**a**); 4 (**b**); 5 (**c**))[24] and $PtCl_2$ were combined in toluene. Chromatographic workups afforded the bis(phosphite) complexes *cis*-$PtCl_2(P(O(CH_2)_{m^*}CH{=}CH_2)_3)_2$ (*cis*-**4a–c**; Scheme 4) as light yellow or colorless oils in 60–95% yields, with $^1J_{PPt}$ values of 5696–5698 Hz. Note that a ligand or complex with a given index has the same number of atoms between the phosphorus atom and the vinyl groups as with the bis(phosphine) complexes *cis*-**1** (e.g., five for *cis*-**1b** and *cis*-**4b**).

Scheme 4. Three-fold Ring Closing Metatheses of *cis*-4a–c: Syntheses of Parachute-like Phosphite Complexes *cis*-5a–c

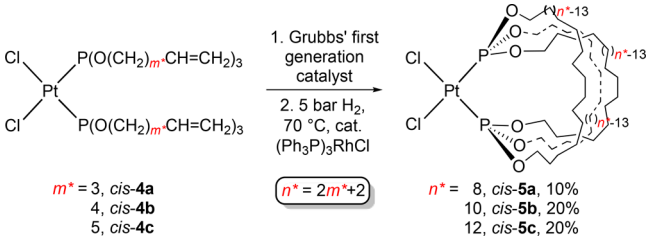

Ring closing metatheses of *cis*-**4a–c** were carried out with Grubbs' first generation catalyst (10–20 mol %) in dilute refluxing CH_2Cl_2 (0.00079–0.00099 M). Hydrogenations were conducted under 5 bar of H_2 using 15–20 mol % of $(Ph_3P)_3RhCl$. As shown in Scheme 4, chromatographic workups gave the target parachute-like dibridgehead diphosphite complexes *cis*-$PtCl_2(P(O(CH_2)_{n^*}O)_3P)$ (*cis*-**5a–c**; $n^* = 2m^* + 2$) as white solids or foams in 10–20% overall yields. A lower homologue of *cis*-**4a**, with one less methylene group in each phosphorus substituent, was also synthesized and similarly reacted. Even with a 25% catalyst loading, ^1H NMR spectra showed a significant fraction of unreacted $CH{=}CH_2$ linkages after 72 h.[21a]

The $^1J_{PPt}$ values of *cis*-**5a–c** ranged from 5721 to 5759 Hz. For all three compounds, two sets of methylene ^{13}C signals with a ca. 2:1 intensity ratio were observed, analogous to the two dibridgehead diphosphine complexes with identical macrocycle

DOI: 10.1021/jacs.8b02846
J. Am. Chem. Soc. 2018, 140, 8463–8478

sizes (*cis*-**2b**,**c**). Importantly, the protons on any CH_2 group of a parachute-like (but not gyroscope-like) complex are diastereotopic. The couplings are never resolved, but as a result, the ^{1}H NMR spectrum of *cis*-**5a** exhibits three well separated OC*HH*′ signals (m, 4H each, $\Delta\delta$ ca. 1.0 ppm). The signals become more closely spaced upon going to *cis*-**5b** ($\Delta\delta$ ca. 0.5 ppm) and *cis*-**5c** (2m, 4H/8H, $\Delta\delta$ ca. 0.15 ppm). The diphosphine complex with the smallest macrocycles, *cis*-**2b**, exhibited three well separated PC*HH*′ signals (m, 4H each, $\Delta\delta$ ca. 0.9 ppm).

2.3. Substitution Reactions. Halide ligands in gyroscope-like complexes are usually quite easily substituted by a variety of nucleophiles.[4−6,16] In all cases, the phosphorus donor atoms remain *trans*. As part of this work, it was not sought to develop an extensive substitution chemistry of parachute-like complexes, but rather to verify that simple displacements can occur and the attendant stereochemistry. The latter is relevant to mechanistic issues described below.

As previously reported,[4b] the gyroscope-like dibridgehead diphosphine complex *trans*-**2c** and Ph_2Zn (3.1 equiv) react over the course of 20 h at room temperature to give the diphenyl complex *trans*-$PtPh_2(P((CH_2)_{14})_3P)$ (*trans*-**6c**) in 61% yield after workup. As shown in Scheme 5, analogous reactions of

Scheme 5. Substitution Reactions of Parachute-like Complexes

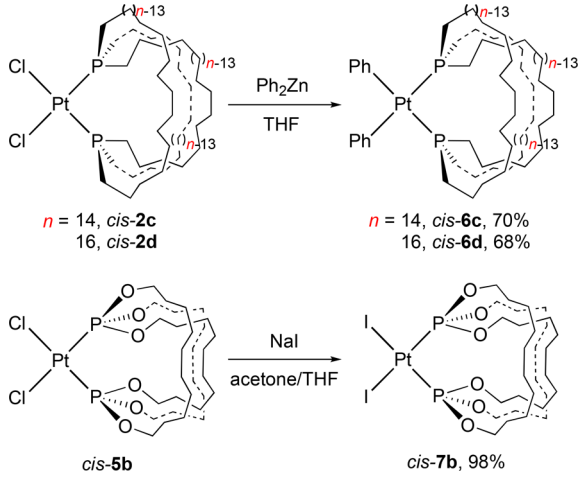

parachute-like *cis*-**2c**,**d** and Ph_2Zn (18 h) gave *cis*-**6c**,**d** as white solids in 68−70% yields. Similarly, a reaction of the dibridgehead diphosphite complex *cis*-**5b** and NaI (4.0 equiv) gave the diiodide complex *cis*-**7b** (Scheme 5) as a yellow solid in 98% yield. The NMR spectra of both substitution products exhibited the general features noted in the precursors above. In contrast to the situation with *trans*-**6c**,[4b] there was no sign of restricted rotation about the Pt−C_{ipso} bond on the NMR time scale with *cis*-**6c**.

2.4. Crystal Structures. Although all of the structures assigned above seemed quite secure based upon spectroscopic properties, it was still sought to crystallographically characterize as many complexes as possible in order to help define the range of accessible macrocycle conformations. Thus, crystals of *cis*-**1f**, *cis*-**2c**,**d**,**f**, *cis*-**6c**, and *cis*-**5a**,**b** were grown as described in the SI. X-ray data were collected, and the structures were determined, as summarized in Table s1 and the SI. The molecular structures are depicted in Figures 2−8. Key bond lengths and angles are given in Table 1. All of these are very close to those of related platinum(II) complexes, but the averages are valuable for certain structural analyses below.

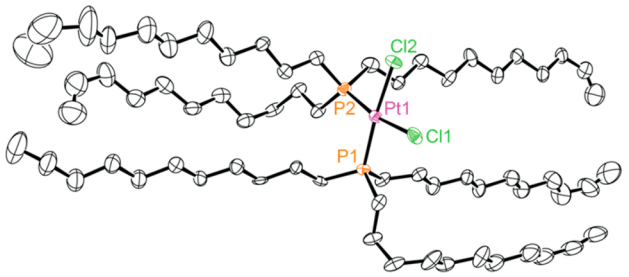

Figure 2. Thermal ellipsoid plot (50% probability) of *cis*-**1f**.

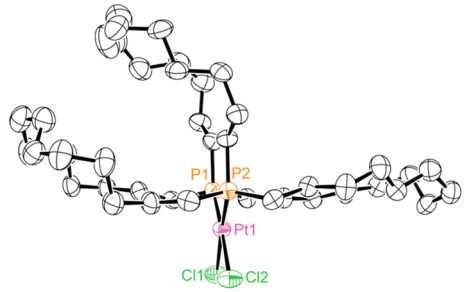

Figure 3. Thermal ellipsoid plot (50% probability) of *cis*-**2c**.

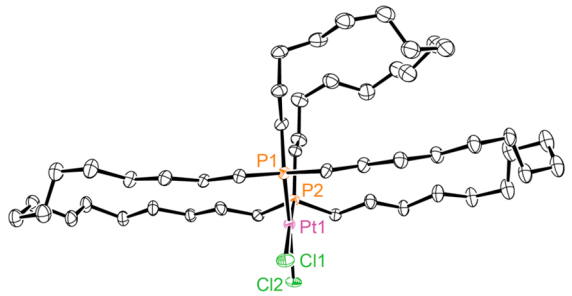

Figure 4. Thermal ellipsoid plot (50% probability) of one of the two independent molecules of *cis*-**2d** in the crystal lattice.

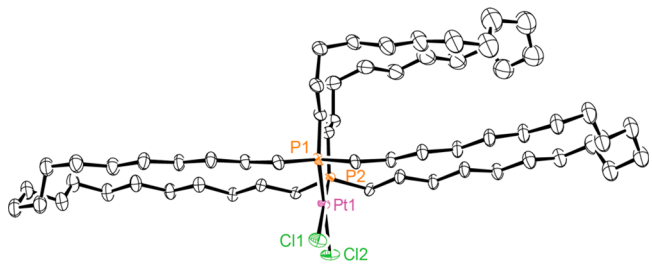

Figure 5. Thermal ellipsoid plot (50% probability) of one of the two independent molecules of *cis*-**2f** in the crystal lattice.

With *cis*-**2d**,**f** and *cis*-**5a**, two independent molecules were present in the unit cell. Those of *cis*-**2d**,**f** were conformationally similar; over all four atom segments in all three macrocycles, the *gauche*/*anti* sense differed in only three linkages. For the independent molecules of *cis*-**5a**, the macrocycles that were perpendicular to the metal coordination plane showed several points of difference. Complex *cis*-**5b** exhibited a C_2 symmetry axis that passed through the platinum atom and bisected the Cl−Pt−Cl angle. Additional structural features are interpreted in Discussion, section 3.

2.5. Thermolyses. Thermal equilibrations of isomeric gyroscope and parachute-like complexes were attempted. An NMR tube was charged with a *o*-$C_6H_4Cl_2$ (*o*-dichlorobenzene) solution of *cis*-**2c**, which features 17-membered macrocycles, and kept at

DOI: 10.1021/jacs.8b02846
J. Am. Chem. Soc. 2018, 140, 8463−8478

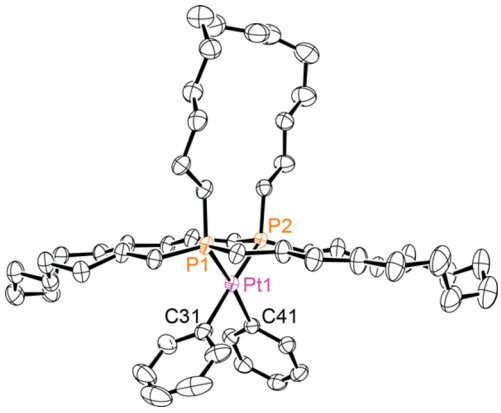

Figure 6. Thermal ellipsoid plot (50% probability) of *cis*-**6c**.

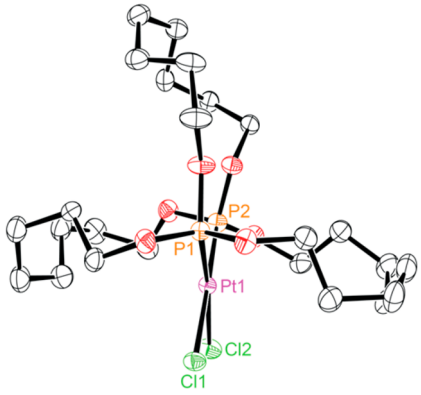

Figure 7. Thermal ellipsoid plot (50% probability) of one of the two independent molecules of *cis*-**5a** in the crystal lattice.

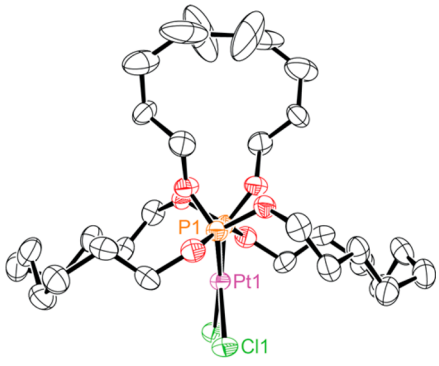

Figure 8. Thermal ellipsoid plot (50% probability) of *cis*-**5b**.

185 °C. As shown by the $^{31}P\{^{1}H\}$ NMR spectra in Figure 9, clean isomerization to *trans*-**2c** gradually took place. The *trans*/*cis* ratio plateaued at 89:11 after 5−6 d (6 d spectrum not depicted). An *o*-$C_6H_4Cl_2$ solution of *trans*-**2c** gave 8% isomerization to *cis*-**2c** after 14 h at 180 °C.

Similar experiments were conducted with C_6D_5Br solutions of **2c**,**g**. No isomerizations were observed with *trans*-**2c**,**g** after 48 h at 150 °C. However, *cis*-**2c**,**g** underwent reactions. As shown in Figure 10, after 1 d, the larger 25-membered macrocycle *cis*-**2g** gave a 74:7:19 mixture of *trans*-**2g**, *cis*-**2g**, and a species tentatively assigned as an oligomer. After another day, the proportion of oligomer had increased slightly (65:6:29).

Interestingly, *cis*-**2c** gave a somewhat slower isomerization (1 d, 16:78:6 *trans*/*cis*/oligomer; 2 d, 22:62:16), although the rate was faster than in *o*-$C_6H_4Cl_2$ at 185 °C. As further detailed in the SI and Figure s5, continued heating at 185 °C gave a significant amount of the previously characterized gyroscope-like *dibromide* complex *trans*-$PtBr_2(P((CH_2)_{14})_3P)$ (2.94 ppm; 22:<1:48:30 *trans*/*cis*/oligomer/dibromide after 3 d).[4b,25]

The preceding experiments indicate that *trans*-**2c**,**g** are thermodynamically more stable than *cis*-**2c**,**g**, with the equilibrium ratio for **2c** being ca. 90:10 (*o*-$C_6H_4Cl_2$, 180−185 °C). DSC analyses of *cis*-**2c** showed an endotherm at 200 °C, nearly coincident with the physically observable melting point at 210 °C. However, no exotherm, which would be expected for an isomerizetion, was noted. Perhaps the barrier is lower in solution than the solid state. TGA data showed an onset of mass loss close to the melting point, suggesting some concomitant decomposition.

In a similar experiment, an NMR tube was charged with a *o*-$C_6H_4Cl_2$ solution of the parachute-like dibridgehead diphosphite complex *cis*-**5b**. No reaction occurred after 1 d at 100 °C or another 2 d at 185 °C, as assayed by $^{31}P\{^{1}H\}$ NMR. When the sample was warmed to 200 °C, numerous decomposition products formed.

2.6. Dynamic Properties. The parachute-like complexes that exhibited two sets of methylene ^{13}C NMR signals (*cis*-**2b−d**, *cis*-**5a−c**) featured smaller macrocycles. Thus, those that exhibited one set of signals (*cis*-**2e−g**) were provisionally assumed to undergo rapid "jump rope" exchange of the methylene bridges per Figure 1. Nonetheless, this interpretation would be strengthened if both regimes could be established for a single complex and activation parameters acquired. Accordingly, samples giving two sets of signals were heated and those giving one set of signals were cooled in hopes of observing coalescence/decoalescence phenomena.

As shown in Figures 11 and s2 (SI), when C_6D_5Br solutions of *cis*-**2d**, which features 19-membered macrocycles, were warmed, the two sets of methylene ^{13}C NMR signals coalesced. As previously observed with gyroscope-like complexes, the chemical shifts were somewhat temperature dependent.[3,7b] This presumably reflects changes in relative populations of macrocycle conformations (each distinguished by a unique set of chemical shifts) as a result of differential entropies. In contrast, the $^{1}J_{PPt}$ value, another potentially sensitive probe, was essentially temperature independent (3529 to 3519 Hz, 25 to 100 °C).

The line shapes of the coalescing signals in Figure 11 were simulated using gNMR,[26] and the rate constants were determined at each temperature. An Eyring plot utilizing these rate constants (Figure s3, SI) afforded $\Delta H^{\ddagger}$, $\Delta S^{\ddagger}$, and $\Delta G^{\ddagger}_{298K}$ values of 7.8 kcal/mol, −27.9 eu, and 16.1 kcal/mol for the process rendering the methylene signals equivalent. As further analyzed below, one would expect a highly negative $\Delta S^{\ddagger}$ for the conformationally restricted transition state **III** in Figure 1.

When C_6D_5Br solutions of *cis*-**2c** or *cis*-**6d**, which feature smaller 17-membered macrocycles or larger phenyl ligands, respectively, were heated to 120−100 °C, no coalescence of methylene ^{13}C NMR signals was observed (Figures s1 and s4). With *cis*-**2c**, this allowed a lower limit of 19.6 kcal/mol ($\Delta G^{\ddagger}_{393K}$) to be set for any process capable of rendering the methylene groups equivalent, as derived in the SI. When CD_2Cl_2 solutions of *cis*-**2e**, which features larger 21-membered macrocycles and a single set of methylene ^{13}C NMR signals, were cooled to −80 °C, no decoalescence was observed.

2.7. Attempted Extension to Octahedral Rhenium Complexes. The ring closing metatheses to give square planar gyroscope-like complexes in Scheme 1 are easily extended to trigonal bipyramidal and octahedral coordination geometries.[3a,b,c,6,7b] Thus, we were curious whether the routes to parachute-like complexes in Schemes 2 and 4 could similarly be applied to trigonal bipyramidal or octahedral educts.

DOI: 10.1021/jacs.8b02846
J. Am. Chem. Soc. 2018, 140, 8463−8478

Table 1. Key Crystallographic Bond Lengths [Å] and Angles [deg]

	cis-**1f**	*cis*-**2c**	*cis*-**2d**[a]	*cis*-**2f**[a]	*cis*-**6c**	*cis*-**5a**[a]	*cis*-**5a**[a]	*cis*-**5b**[b]
Pt–P	2.256(2)	2.2507(14)	2.2506(18)/2.258(2)	2.245(3)/2.250(3)	2.3188(6)	2.2138(7)	2.2167(7)	2.209(3)
	2.263(2)	2.2563(14)	2.248(2)/2.2492(19)	2.243(3)/2.231(3)	2.3204(6)	2.2248(8)	2.2191(8)	
Pt–X[c]	2.352(2)	2.3661(14)	2.351(2)/2.360(2)	2.347(3)/2.345(3)	2.056(3)	2.3509(7)	2.3455(7)	2.352(3)[d]
	2.354(2)	2.3689(14)	2.774(19)/2.371(2)	2.365(3)/2.373(3)	2.070(3)	2.3548(7)[d]	2.3492(7)[d]	
P–Pt–P	100.27(9)	104.37(5)	104.59(7)/104.70(7)	104.66(11)/104.29(11)	105.00(2)	100.11(3)	99.37(3)	91.07(16)
P–Pt–X	83.94(9)	83.23(5)	83.42(7)/83.66(7)	83.52(10)/83.17(11)	85.66(8)	82.84(3)	83.99(3)	91.17(13)
	90.72(8)	84.98(5)	84.17(7)/84.23(7)	84.08(11)/84.13(11)	86.10(7)	88.73(3)	89.38(3)	
	168.69(8)	170.65(5)	171.22(7)/171.07(7)	171.22(10)/171.36(11)	168.08(8)	170.85(3)	171.15(3)	172.7(1)
	174.59(8)	172.35(5)	171.97(7)/171.61(7)	171.66(11)/172.23(11)	168.45(7)	176.87(3)	175.77(3)	
X–Pt–X	84.94(9)	87.42(6)	87.82(7)/87.42(7)	87.77(10)/88.51(11)	83.61(10)	88.29(3)	87.21(3)	87.5(2)

[a]Values for the two independent molecules in the unit cell. [b]A C_2 symmetry axis renders the Pt–P and Pt–X bond lengths and other parameters equivalent. [c]Distances from platinum to the ligating atoms of the non-phosphine ligands. [d]The phosphorus–oxygen and oxygen–carbon bond lengths in *cis*-**5a,b** fall into the ranges 1.557(2)–1.593(2) Å and 1.432(17)–1.475(4) Å.

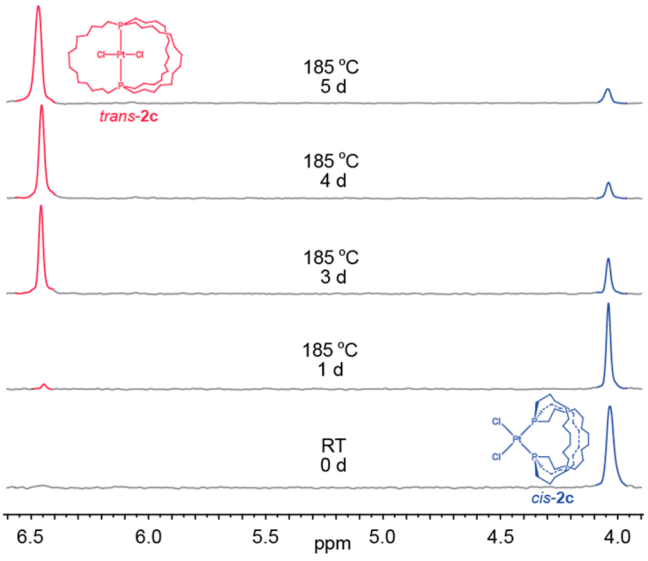

Figure 9. Thermolysis of *cis*-**2c** in *o*-$C_6H_4Cl_2$ at 185 °C; $^{31}P\{^1H\}$ NMR data.

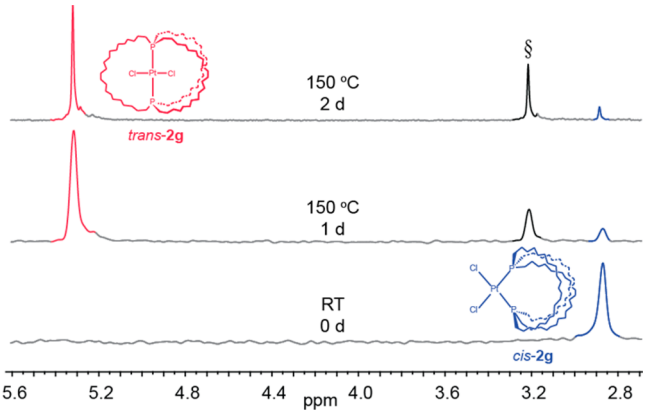

Figure 10. Thermolysis of *cis*-**2g** in C_6D_5Br at 150 °C; $^{31}P\{^1H\}$ NMR data (§ denotes an unidentified substance believed to be oligomer).

Accordingly, the rhenium halide complexes $ReX(CO)_5$ (X = Cl, Br) and the olefinic phosphine $P((CH_2)_6CH{=}CH_2)_3$ (2.0 equiv) were combined in C_6H_5Cl at 60–80 °C. Workups gave the *cis* bis(phosphine) complexes *fac*-$ReX(CO)_3(P((CH_2)_6CH{=}CH_2)_3)_2$ (X = Cl, *fac*-**10c**; Br, *fac*-**11c**) in 43–67% yields. As shown in Scheme 6, the thermolysis of *fac*-**11c** in C_6H_5Cl at 140 °C afforded the previously characterized[6a] isomer *mer,trans*-**11c** in 89% yield. Many earlier studies have shown that *mer,trans* isomers of rhenium tricarbonyl bis(phosphine) halide complexes are more stable than *fac* isomers.[27] As noted previously, when *mer,trans*-**11c** is subjected to the standard metathesis/hydrogenation conditions, the corresponding gyroscope-like complex *mer,trans*-$ReBr(CO)_3(P((CH_2)_{14})_3P)$ (*mer,trans*-**12c**; Scheme 6) can be isolated in 37% yield.[6a]

In procedures parallel to those in Schemes 2 and 4, *fac*-**10c** and *fac*-**11c** were treated with Grubbs' first generation catalyst and then H_2/PtO_2. As shown in Scheme 6, workups gave products derived from a combination of *interligand* and *intraligand* metatheses, *fac*-**12′c** and *fac*-**13′c**, in 39% and 15% overall yields, respectively. The parachute-like complexes *fac*-**12c** and *fac*-**13c** were not detected; due to their lower symmetry vs *cis*-**2**, three sets of methylene ^{13}C NMR signals, one for each macrocycle, would be expected. Interestingly, mass spectra of the crude metathesis product derived from *fac*-**10c** exhibited a number of dirhenium ions (e.g., $2M^+ - 3CO$, 100%).

As a further check of structure, *fac*-**12′c** and *fac*-**13′c** were thermolyzed in C_6H_5Cl at 130–140 °C. Similar to the result with *fac*-**11c**, *mer,trans*-**12′c** and *mer,trans*-**13′c** were isolated in 17–22% yields. The complex *mer,trans*-**12′c** had been independently synthesized earlier (byproduct accompanying *mer,trans*-**12c**), as had homologues of *mer,trans*-**13′c** with larger macrocycles.[6a] Thermolyses of the target complexes, *fac*-**12c** and *fac*-**13c**, would have given the known gyroscope-like complexes *mer,trans*-**12c** and *mer,trans*-**13c**.[6a]

2.8. Computational Studies. Further insight was sought regarding the relative stabilities of the various types of isomeric species encountered above. Thus, DFT calculations, including dispersion corrections, were carried out. This was followed by molecular dynamics annealing simulations to maximize the likelihood of correctly identifying the lowest energy conformer. This output was further optimized by additional DFT calculations. As shown in Figure s9 (SI), the dispersion corrections gave structures that more closely modeled those in the crystal structures.

The relative gas phase stabilities of the parachute- and gyroscope-like complexes *cis*-**2** and *trans*-**2** are illustrated as a function of macrocycle size in Figure 12. As one goes from 13- to 25-membered macrocycles (or 10 (**a**) to 22 (**g**) methylene groups per bridge), the gyroscope-like complexes range from 5.1 to 9.2 kcal/mol more stable, consistent with the trends established for **2c,g** in haloarenes in Figures 9 and 10. However, the energy differences do not vary monotonically. Rather, there is an "even/odd" alternation with respect to $n/2$ (odd, −9.2 to −8.5 kcal/mol; even, −5.8 to −5.1 kcal/mol). No attempt has been made to elucidate a basis for this phenomenon. However, it may be coupled to

DOI: 10.1021/jacs.8b02846
J. Am. Chem. Soc. 2018, 140, 8463–8478

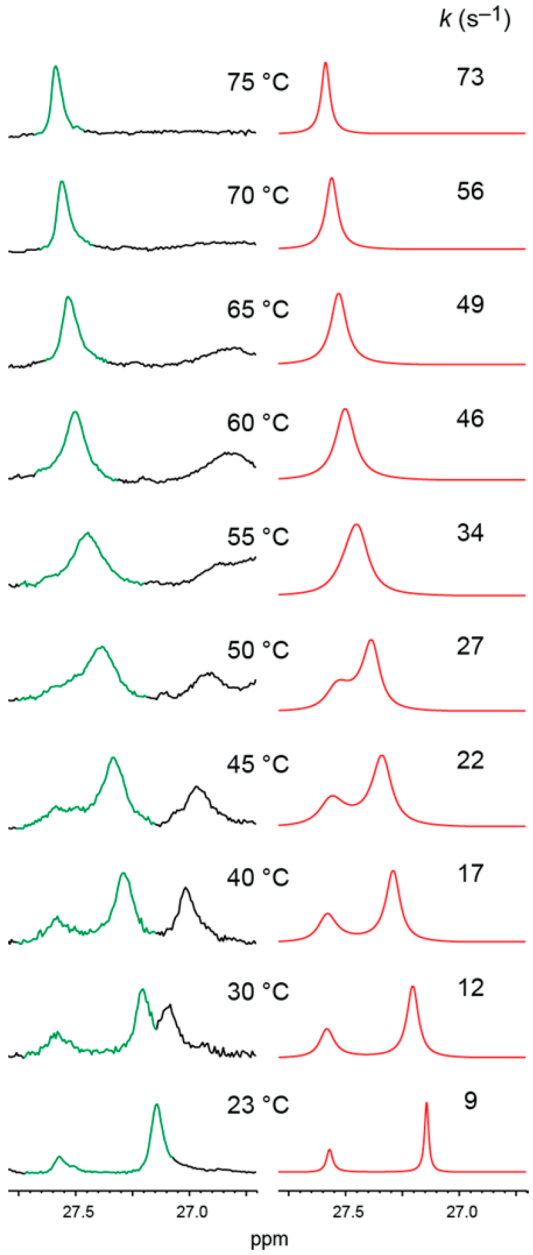

Figure 11. Partial $^{13}C\{^{1}H\}$ NMR spectra of *cis*-**2d** (C_6D_5Br) as a function of temperature. Each spectrum (left) is paired with simulated line shapes for the signals of interest (right; compare red and green traces).

conformational features of the macrocycles. Physical properties that alternate with even/odd methylene chain lengths have abundant precedent.[28]

Figure 12 also displays the relative energies of the alternative cyclization products *trans*-**2′a**–**g** (Scheme 1) and *cis*-**2′a**–**g** (Scheme 2). The former is more stable for all macrocycle sizes. In both cases, the complexes with the two smallest macrocycle sizes, **2′a**,**b**, are considerably higher in energy, also as compared to gyroscope- and parachute-like **2a**,**b**. This presumably reflects ring strain associated with the monophosphacycles. The energies of **2′a**–**g** generally decrease with increasing macrocycle size, although not monotonically. Interestingly, *trans*-**2′f**,**g**, which feature the two largest macrocycle sizes, are computed to be more stable than gyroscope-like *trans*-**2f**,**g** (−8.5 to −3.5 kcal/mol).

Data for the parachute- and gyroscope-like phosphite complexes *cis*-**5a**–**g** and *trans*-**5a**–**g** are also provided in Figure 12 (right). Now the former are computed to be more stable, consistent with (1) the preferred geometry for acyclic bis(phosphite) platinum dichloride complexes and (2) the absence of any thermal isomerization of *cis*-**5b**, as noted above. Thus, a metal based electronic effect dominates over any ring strain trends that may be operative with the macrocycles.

Data for the four types of isomeric rhenium complexes in Scheme 6 are provided in Figure 13. Consistent with the thermolyses in Scheme 6, and the direction of equilibrium for a number of related complexes,[27] *mer*,*trans*-**12′c** and *mer*,*trans*-**13′c** were found to be much more stable than *fac*-**12′c** and *fac*-**13′c** (−5.4 to −7.4 kcal/mol). Interestingly, the energies of the previously synthesized gyroscope-like complexes *mer*,*trans*-**12c** and *mer*,*trans*-**13c** were quite close to those of the parachute-like complexes *fac*-**12c** and *fac*-**13c** (≤0.4 kcal/mol). Thus, the latter remain realistic synthetic targets, although the cyclization mode leading to (after hydrogenation) the much less stable *fac*-**12′c** and *fac*-**13′c** is preferred under the conditions of Scheme 6.

3. DISCUSSION

3.1. Syntheses and Structures. Schemes 2 and 4 establish that parachute-like square planar platinum complexes are easily accessed, albeit in modest yields, via 3-fold *interligand* ring closing metatheses of precursors with suitable *cis* olefinic phosphine and phosphite ligands. It also appears that they can be accessed with smaller macrocycles than the corresponding gyroscope-like complexes, as exemplified by *cis*-**5a** (13-membered), *cis*-**5b**, and *cis*-**2b** (both 15-membered). As noted above, attempts to synthesize gyroscope-like square planar complexes with macrocycles of less than 17 atoms have yet to be successful.

It seems likely that Schemes 2 and 4 can be extended to other square planar complexes. However, there appear to be greater restrictions with respect to the metal coordination geometry than for gyroscope-like complexes, as reflected by the failure to access octahedral analogs in Scheme 6. Here, an alternative mode of ring closing metathesis affords *cis* bis(phosphacycle) chelate ligands (*fac*-**12′c** and *fac*-**13′c**). As noted above, related complexes with *trans* spanning chelates, such as *mer*,*trans*-**12′c**, are sometimes found as byproducts in syntheses of octahedral gyroscope-like complexes.[4b,6]

Prior to our work, no aliphatic dibridgehead diphosphines with bridges greater than four atoms had been synthesized, as either complexes or free ligands.[29] Analogous diphosphites were unknown, although macrocyclic aromatic analogs derived from $P(OAr)_3$ units had been reported.[30] This study establishes that such ligands possess incredible flexibility, as illustrated in Scheme 7. Naturally the phosphorus-lone pair vectors can orient collinearly with a 180° angle (**V**), as seen in bimetallic complexes.[31] In the parachute-like complexes *cis*-**2** and *cis*-**4**, these vectors define 90° angles (**VII**). Intermediate geometries such as **VI** should be possible, in which the lone pairs might be directed at a surface or polymetallic assembly. Continued rotation of the vectors leads to gyroscope-like complexes (**VIII**), in which the phosphorus configurations have been inverted relative to **V**. These changes in vector orientations require specific accompanying changes in the conformations of the methylene bridges, processes that will be fully treated in a future paper addressing mechanisms of interconversion of **V** and **VIII**.

The crystal structures determined include parachute-like complexes with 13-, 15-, 17-, 19-, and 23-membered macrocycles. These can be compared to the conformational model in Figure 1, in which the "middle" macrocycle occupies the metal coordination

DOI: 10.1021/jacs.8b02846
J. Am. Chem. Soc. 2018, 140, 8463–8478

Scheme 6. Three-fold Ring Closing Metatheses of the Octahedral Rhenium Complexes *fac*-10c and *fac*-11c and Related Reactions

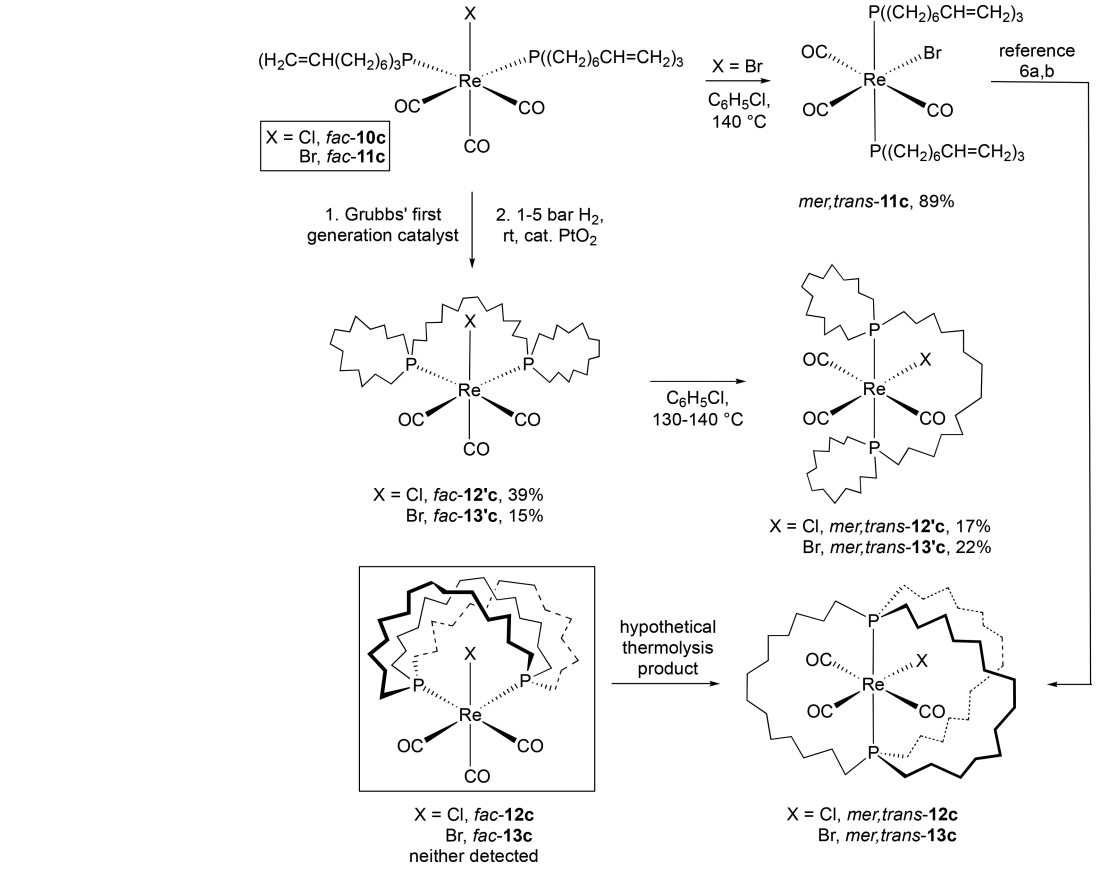

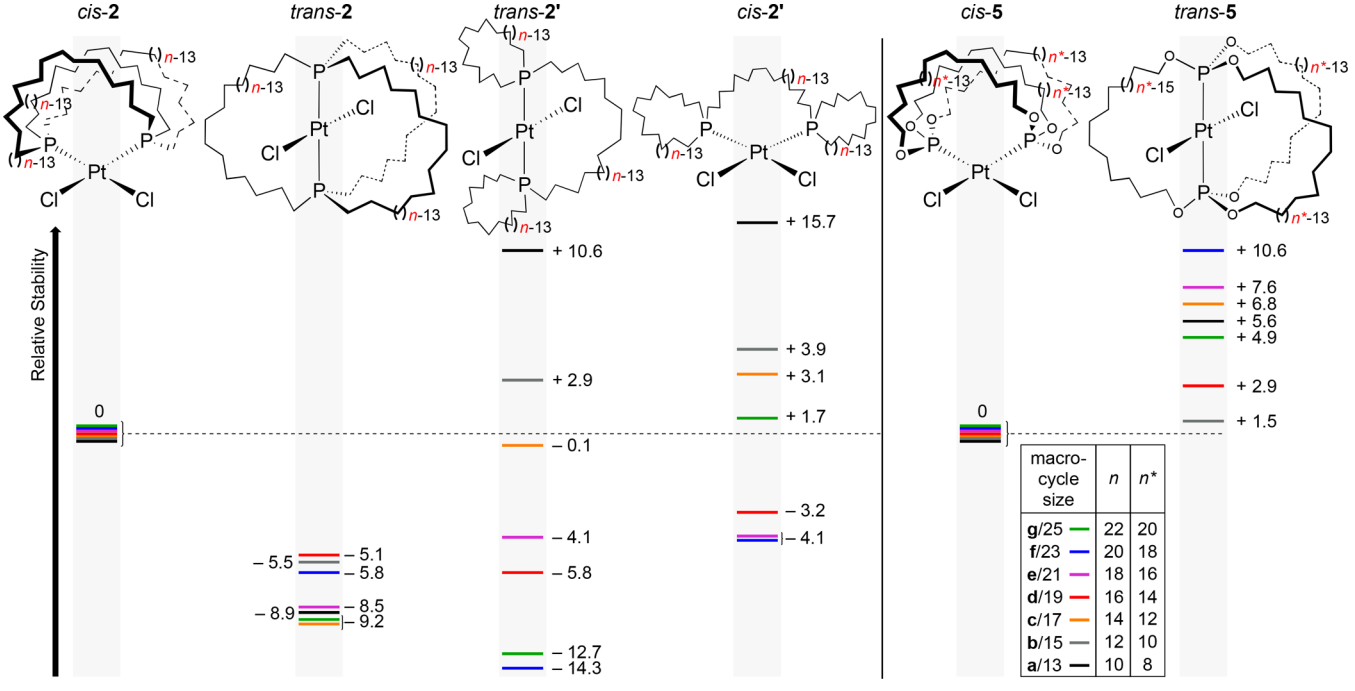

Figure 12. Relative energies (kcal/mol) of isomeric platinum dichloride complexes as computed by DFT and molecular dynamics (gas phase).

plane. This is always the case for the first few atoms emanating from phosphorus. However, as shown in Figures 3–5, the middle macrocycles in *cis*-**2c,d,f** exhibit a subsequent fold or "kink". The other macrocycles adopt approximately perpendicular orientations above and below the coordination plane.

The crystal structure of one precursor to a parachute-like complex, *cis*-**1f**, could be determined. As shown in Figure 2, the spatial distribution of the six vinyl groups is by no means conducive for the required 3-fold *interligand* ring closing alkene metathesis. This is presumably one factor behind the modest yields in

DOI: 10.1021/jacs.8b02846
J. Am. Chem. Soc. 2018, 140, 8463–8478

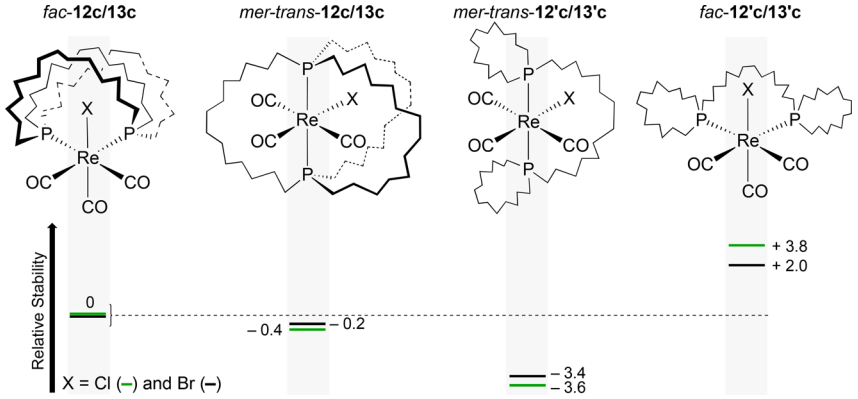

Figure 13. Relative energies (kcal/mol) of isomeric rhenium tris(carbonyl) halide complexes as computed by DFT and molecular dynamics (gas phase).

Scheme 7. Limiting Structures for Macrocyclic Dibridgehead Diphosphorus Ligands

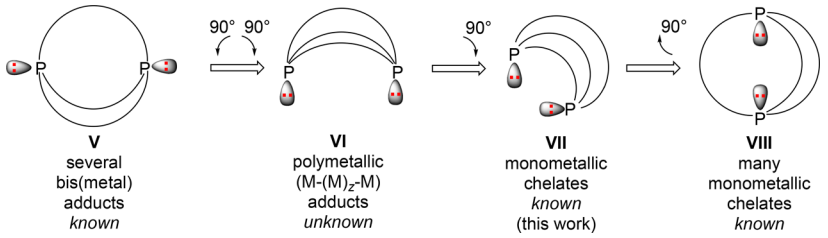

Schemes 2 and 4. In contrast, favorable or "preorganized" conformations have been documented for hexaolefinic educts that give trigonal planar gyroscope-like complexes in quite good yields.[3,7b]

3.2. Dynamic Properties. Dynamic processes in which a macrocycle must rotate or "jump" over another moiety are not unusual.[15,32] However, the 3-fold variant invoked for parachute-like complexes with sufficiently long methylene bridges (Figure 1) is to our knowledge unprecedented. In the absence of such exchange, the macrocycles above and below the coordination plane must give methylene ^{13}C NMR signals distinct from those of the macrocycle in the coordination plane.

The "jump rope" process requires that the $PtCl_2$ moiety pass through each macrocycle. Although this is accomplished by correlated rotations about the platinum–phosphorus bonds, the phosphorus–phosphorus vector, highlighted in **IX** in Figure 14, provides a valuable reference point for analyzing steric interactions. The two chlorine atoms are 2.88 Å from this vector (average of 16 distances in all independent molecules in crystalline *cis*-**2c,d,f** and *cis*-**5a,b**; see Table 1). When the van der Waals radius of a chlorine atom is added (1.75 Å),[33] an effective "length" or radius of 4.63 Å is obtained.

At the same time, the $PtCl_2$ moiety has "width" or "fatness". The average chlorine–chlorine distance in *cis*-**2c,d,f** and *cis*-**5a,b** is 3.59 Å. When twice the van der Waals radius of a chlorine atom is added, an effective width of 7.09 Å is obtained. The activation barriers reflect the ease with which the cavities of the macrocycles can adapt to these dimensions (4.63 × 7.09 Å).

One approach to gauging the "lengths" of the macrocycles in a given complex is to calculate the distance from the center of the phosphorus–phosphorus vector to the two carbon atoms at the halfway mark of the three macrocycles. These will often, but not always, be the two carbon atoms most distant from the phosphorus–phosphorus midpoint. The six values are averaged (12 for the cases of two independent molecules), and the van der Waals radius of an sp^3 carbon atom is subtracted. As would be expected,

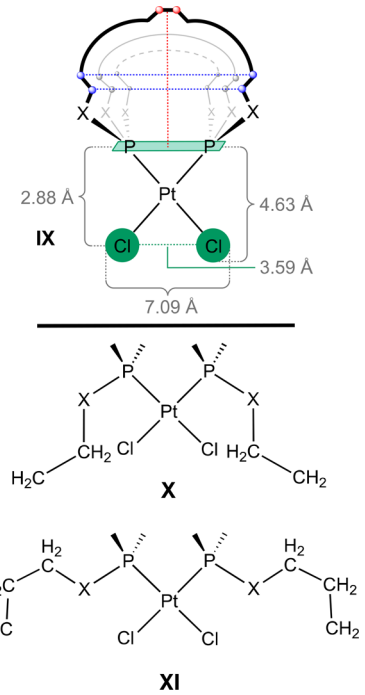

Figure 14. IX: Spatial relationships involving the $PtCl_2$ moiety and macrocycles of *cis*-**2** (X = CH_2) and *cis*-**5** (X = O); parameters that affect the energy barriers for bridge exchange. **X**, **XI**: partial macrocycle conformations corresponding to possible transition states for bridge exchange.

the resulting values ascend in the order *cis*-**5a,b** and *cis*-**2c,d,f** (3.31, 4.04, 5.49, 7.09, 9.49 Å). Thus, *cis*-**2c,d,f** can easily accommodate the 4.63 Å "length" of the $PtCl_2$ moiety, whereas *cis*-**5b** requires a bit of a squeeze.

The effective "width" is another matter. As can be seen in Figures 3, 4, 7, and 8, the P–X–CH_2 and P–X–CH_2–CH_2 groups of each macrocycle will most closely flank the $PtCl_2$

DOI: 10.1021/jacs.8b02846
J. Am. Chem. Soc. 2018, 140, 8463–8478

moiety during the "jump rope" process. It is a simple matter to calculate the distances between the two P−X−CH_2 carbon atoms of a given macrocycle, and the two P−X−CH_2−CH_2 carbon atoms (X = O or CH_2). The three values for a given complex are averaged (six for the cases of two independent molecules), and twice the van der Waals radius of a carbon atom is subtracted. This gives clearances that vary irregularly over a ca. 1 Å range for *cis*-**5a**,**b** and *cis*-**2c**,**d**,**f** (1.67, 2.21, 1.34, 1.78, 1.39 Å for P−X−CH_2; 1.30, 2.31, 2.44, 1.40, 2.08 Å for P−X−CH_2−CH_2). None of these are sufficient to accommodate the "width" of the $PtCl_2$ moiety (7.09 Å).

Hence, the jump rope process must incorporate conformational changes in the macrocycles that constitute significant deviations from the crystal structures. Figure 14 shows two partial conformations that widen the macrocycle cavity (**X** < **XI**). This is accomplished by introducing *anti* four-atom segments, for example, P−X−CH_2−CH_2 in **X** and Pt−P−X−CH_2 and P−X−CH_2−CH_2 in **XI**. These in turn render it more difficult to "close the macrocycle" with the remaining atoms without inducing strain. Thus, the bridges of the smaller macrocycles lack sufficient degrees of freedom, and the activation parameters become prohibitive. Only upon reaching *cis*-**2d**, which features 19-membered macrocycles, does exchange become observable on the NMR time scale. The significantly negative $\Delta S^{\ddagger}$ (−27.9 eu) is consistent with highly ordered macrocycle conformations such as **X** or **XI** in the transition state. Alternative mechanisms involving the dissociation of a phosphorus atom can be excluded as all of the complexes retain $^1J_{PPt}$ values in the rapid exchange limit (e.g., *cis*-**2e**−**g** at room temperature or *cis*-**2d** at 75−100 °C).

3.3. Relative Isomer Stabilities. It is clear from the thermolysis experiments (Figures 9, 10, s5) that the gyroscope-like platinum dibridgehead diphosphine complexes *trans*-**2c**,**g** are more stable than the parachute-like analogs *cis*-**2c**,**g**, at least in low polarity solvents such as haloarenes. The gas phase computational data (Figure 12) confirm the generality of the stability trend for all macrocycle sizes that have been synthetically accessed (*trans*-**2b**−**g** > *cis*-**2b**−**g**). Given the extreme temperatures required for equilibration (150−185 °C), it can be concluded that *cis* isomers are not intermediates in the complexation of MCl_2 by the free dibridgehead diphosphines **3** (Scheme 3), a key step in their application as "container molecules".[17]

The computational data are of particular value in cases where authentic samples of both *cis* and *trans* complexes are lacking, such as with the dibridgehead diphosphite complexes *cis*-**5a**−**c**. Currently, there is no way to access suitable precursors to the *trans* isomers. As noted above, the reversal of the relative stabilities of parachute- and gyroscope-like complexes with the diphosphite complexes **5a**−**g** as compared to diphosphine complexes **2a**−**g** underscores the importance of electronic effects. Indeed, preliminary computational results show that with certain small ancillary ligands, parachute-like diphosphine complexes can become more stable. These data, which are beyond the scope of the present study, will be presented in a future full paper.[34]

Some issues that the computational data do *not* address deserve note. As emphasized in past studies,[3b,4b,6b] our ring closing metathesis reactions are generally under kinetic control. Thus, the ratios of constitutional isomers such as *trans*-**2** and *trans*-**2′** (Scheme 1), *cis*-**2** and *cis*-**2′** (Scheme 2), or *fac*-**12c** and *fac*-**12′c** (Scheme 6) reflect the ratios of the precursor cycloalkenes (prior to hydrogenation). These are always complex mixtures of *Z*/*E* isomers of undefined ratios, and should not automatically correlate to any distribution computed from the relative energies of the saturated products.

Nucleophilic substitutions of chloride ligands in both parachute- and gyroscope-type platinum complexes (e.g., Scheme 5) take place without geometric isomerization and therefore fit the rigorous definition of stereospecific reactions.[35] This leads in turn to a number of conclusions, for example, that the diphenyl complex *cis*-**6c** is not an intermediate in the synthesis of *trans*-**6c**, and vice versa. Finally, mention should be made of related studies involving the relative stabilities of *cis*/*trans* MCl_2 (M = Pt, Pd) adducts of monophosphines as well as diphosphines capable of both *cis* and *trans* coordination.[36]

3.4. Conclusion. This study has established the general accessibility of square planar platinum dichloride complexes with *cis* coordinated dibridgehead *diphosphine* and *diphosphite* ligands, albeit in modest yields. When the three macrocycles in these "parachute-like" species are sufficiently large, they can sequentially "jump" over the $PtCl_2$ moiety in a dynamic process that appears to be topologically unprecedented, and reminiscent of a triple axel. Isomeric *trans* dibridgehead *diphosphine* complexes, termed "gyroscope-like", have been synthesized earlier and are thermodynamically more stable. Isomeric *trans* dibridgehead *diphosphite* complexes cannot presently be accessed, but computational data indicate that they are *less* stable. Results with octahedral rhenium complexes suggest that it is unlikely that parachute-like complexes will be accessible with higher coordination geometries. The preceding data also eliminate certain mechanistic variants from various phenomena involving gyroscope-like platinum complexes, simplifying the interpretation of their chemistry.

4. EXPERIMENTAL SECTION

4.1. General. Reactions were conducted under inert atmospheres using standard Schlenk techniques unless noted. DSC and TGA data were recorded with a Mettler-Toledo DSC821 instrument and treated by standard methods.[37] Additional data are supplied in the SI.

*4.1.1. Metathesis of cis-**1b**.* A Schlenk flask was charged with *cis*-**1b** (0.438 g, 0.481 mmol),[14] Grubbs' first generation catalyst (0.0274 g, 0.0329 mmol, 7.5 mol %), and CH_2Cl_2 (320 mL; the resulting solution is 0.0015 M in *cis*-**1b**) and fitted with a condenser. The solution was refluxed with stirring (12 h). The solvent was removed by oil pump vacuum, and CH_2Cl_2 was added. The sample was passed through a short pad of neutral alumina, rinsing with CH_2Cl_2. The solvent was removed from the filtrate by oil pump vacuum to give metathesized *cis*-**1b** (0.158 g, 0.191 mmol, 40%) as a light brown solid. NMR ($CDCl_3$, δ/ppm): $^{31}P\{^1H\}$ (162 MHz) 7.6 (s, 26%), 6.9 (s, 39%), 5.4 (s, 18%), 4.1 (s, 17%).

*4.1.2. cis-$PtCl_2(P((CH_2)_{12})_3P)$ (cis-**2b**).* A Fischer−Porter bottle was charged with metathesized *cis*-**1b** (0.150 g, 0.181 mmol), $(Ph_3P)_3RhCl$ (0.0252 g, 0.0272 mmol, 15 mol %), CH_2Cl_2 (20 mL), and H_2 (5 bar). The solution was stirred (72 h). The solvent was removed by oil pump vacuum, and CH_2Cl_2 was added. The sample was passed through a short pad of neutral alumina, rinsing with CH_2Cl_2. Two fractions were collected. The solvents were removed by oil pump vacuum. The second fraction gave *cis*-**2b** (0.023 g, 0.028 mmol, 15%) as a light brown solid, mp (capillary) 260 °C. TGA: onset of mass loss, 109 °C (8%). Anal. Calcd (%) for $C_{36}H_{72}Cl_2P_2Pt$ (832.89): C, 51.92; H, 8.71. Found: C, 51.22; H, 8.48.[38]

NMR ($CDCl_3$, δ/ppm): ^1H (400 MHz) 2.62−2.60 (br m, 4H, PCH_2), 2.05−2.03 (br s, 4H, PCH_2), 1.72 (br s, 4H, PCH_2), 1.65−1.24 (m, 60H, remaining CH_2); $^{13}C\{^1H\}$ (100 MHz)[39] 30.1 (virtual t,[41] J_{CP} = 8.4 Hz, 4C, $PCH_2CH_2CH_2$), 29.7 (virtual t,[41] J_{CP} = 5.4 Hz, 2C, $PCH_2CH_2CH_2$), 27.5 (s, 4C, CH_2), 27.1 (s, 2C, CH_2), 26.7 (s, 2C, CH_2), 26.2 (s, 2C, CH_2), 25.7 (s, 4C, CH_2), 25.2 (s, 4C, CH_2), 24.7 (s, 4C, PCH_2CH_2), 24.5 (br s, 2C, PCH_2CH_2), 24.1 (br s, 4C, PCH_2), 22.9 (br s, 2C, PCH_2); $^{31}P\{^1H\}$ (162 MHz) 7.4 (s, $^1J_{PPt}$ = 3568 Hz[42]). MS:[43] 832 (M^+, 20%), 797 (M^+ − Cl, 100%), 759 (M^+ − 2Cl, 85%).

*4.1.3. Metathesis of cis-**1c**.* Grubbs' first generation catalyst (0.033 g, 0.040 mmol, 10 mol %), *cis*-**1c** (0.2000 g, 0.2009 mmol),[14] and CH_2Cl_2 (200 mL; the resulting solution is 0.0010 M in *cis*-**1c**) were combined in

DOI: 10.1021/jacs.8b02846
J. Am. Chem. Soc. 2018, 140, 8463−8478

a procedure analogous to that for *cis*-**1b**. An identical workup gave metathesized *cis*-**1c** (0.098 g, 0.107 mmol, 53%) as a white solid. NMR ($CDCl_3$, δ/ppm): $^{31}P\{^1H\}$ (162 MHz) 9.8 (s, 53%), 9.5 (s, 33%), 8.4 (s, 7%), 8.0 (s, 7%).

*4.1.4. cis-$PtCl_2(P((CH_2)_{14})_3P)$ (cis-**2c**).* Metathesized *cis*-**1c** (0.0980 g, 0.108 mmol), $(Ph_3P)_3RhCl$ (0.0148 g, 0.0160 mmol, 15 mol %), toluene (20 mL), and H_2 (5 bar) were combined in a procedure analogous to that for *cis*-**2b**. An identical workup gave *cis*-**2c** (0.0740 g, 0.0807 mmol, 75%) as a light brown solid, mp (capillary) 210 °C. DSC ($T_i/T_e/T_p/T_c/T_f$):[37] 140.2/200.2/211.1/214.9/218.4 (endotherm) °C. TGA: onset of mass loss, 204 °C. Anal. Calcd (%) for $C_{42}H_{84}Cl_2P_2Pt$ (917.05): C, 55.01; H, 9.23. Found: C, 52.48; H, 9.17.[38]

NMR (CD_2Cl_2, δ/ppm): ^1H (400 MHz) 2.58−2.55 (br m, 4H, PCH_2), 1.84−1.78 (br m, 8H, PCH_2), 1.46−1.26 (br m, 72H, remaining CH_2); $^{13}C\{^1H\}$ (100 MHz)[39] 31.0 (virtual t,[41] J_{CP} = 4.6 Hz, 2C, $PCH_2CH_2CH_2$), 30.6 (virtual t,[41] J_{CP} = 7.6 Hz, 4C, $PCH_2CH_2CH_2$), 28.7 (s, 4C, CH_2), 27.7 (s, 2C, CH_2), 27.6 (s, 2C, CH_2), 27.34 (s, 4C, CH_2), 27.25 (s, 8C, CH_2), 26.6 (s, 4C, CH_2), 25.4 (s, 4C, PCH_2CH_2), 25.2 (br s, 2C, PCH_2CH_2), 24.7 (br s, 4C, PCH_2), 23.7 (br s, 2C, PCH_2); $^{31}P\{^1H\}$ (162 MHz) 5.3 (s, $^1J_{PPt}$ = 3543 Hz[42]). MS:[43] 916 (M^+, 20%), 882 ($M^+ - Cl$, 40%), 844 ($M^+ - 2Cl$, 100%).

*4.1.5. cis-$PtCl_2(P((CH_2)_{16})_3P)$ (cis-**2d**).* Grubbs' first generation catalyst (0.0445 g, 0.0541 mmol, 12 mol %), *cis*-**1d** (0.4868 g, 0.451 mmol),[14] and CH_2Cl_2 (750 mL; the resulting solution is 0.00060 M in *cis*-**1d**) were combined in a procedure analogous to that for the metathesis of *cis*-**1b**. After the alumina filtration step, the CH_2Cl_2 filtrate, PtO_2 (0.0236 g, 0.104 mmol), and H_2 (5 bar) were combined in a Fischer−Porter bottle. A reaction and workup analogous to that for *cis*-**2b** gave *cis*-**2d** (0.0772 g, 0.077 mmol, 17%) as a white solid, mp (capillary) 159−161 °C. Anal. Calcd (%) for $C_{48}H_{96}Cl_2P_2Pt$ (1001.23): C, 57.58; H, 9.66. Found: C, 57.73; H, 9.77.

NMR ($CDCl_3$, δ/ppm): ^1H (500 MHz) 2.68−1.51 (m, 12H, PCH_2), 2.01−1.88 (m, 12H, PCH_2CH_2), 1.78−1.70 (m, 12H, $PCH_2CH_2CH_2$), 1.35−1.20 (m, 60H, remaining CH_2); $^{13}C\{^1H\}$ (126 MHz)[39] 31.24 (virtual t,[41] J_{CP} = 4.6 Hz, 2C, $PCH_2CH_2CH_2$), 31.16 (virtual t,[41] J_{CP} = 7.6 Hz, 4C, $PCH_2CH_2CH_2$), 29.2 (s, 4C, CH_2), 28.6 (s, 2C, CH_2), 28.4 (s, 2C, CH_2), 28.3 (s, 4C, CH_2), 27.7 (s, 4C, CH_2), 27.4 (s, 2C, CH_2), 27.0 (s, 2C, CH_2), 26.8 (s, 2C, CH_2), 26.5 (s, 4C, CH_2), 26.0 (s, 4C, CH_2), 25.8 (s, 4C, PCH_2CH_2), 24.9 (br s, 2C, PCH_2CH_2), 24.5 (br s, 4C, PCH_2), 23.8 (br s, 2C, PCH_2); $^{31}P\{^1H\}$ (202 MHz) 4.35 (s, $^1J_{PPt}$ = 3550 Hz[42]). **IR** (cm^{-1}, powder film): 2930 (s), 2844 (m), 1730 (m), 1461 (m), 1265 (m), 1074 (m), 726 (m).

*4.1.6. Metathesis of cis-**1e**.* Grubbs' first generation catalyst (0.0213 g, 0.0258 mmol, 12.0 mol %), *cis*-**1e** (0.251 g, 0.215 mmol),[14] and CH_2Cl_2 (215 mL; the resulting solution is 0.0010 M in *cis*-**1e**) were combined in a procedure analogous to that for *cis*-**1b**. An identical workup gave metathesized *cis*-**1e** (0.119 g, 0.110 mmol, 51%) as a white solid. NMR ($CDCl_3$, δ/ppm): $^{31}P\{^1H\}$ (162 MHz) 7.6 (s, 47%), 7.3 (s, 35%), 6.9 (s, 7%), 3.8 (s, 11%).

*4.1.7. cis-$PtCl_2(P(CH_2)_{18})_3P)$ (cis-**2e**).* Metathesized *cis*-**1e** (0.180 g, 0.167 mmol), $(Ph_3P)_3RhCl$ (0.023 g, 0.025 mmol, 15 mol %), CH_2Cl_2 (20 mL), and H_2 (5 bar) were combined in a procedure analogous to that for *cis*-**2b**. An identical workup gave *cis*-**2e** (0.033 g, 0.030 mmol, 18%) as a light brown solid, mp (capillary) 185 °C. DSC ($T_i/T_e/T_p/T_c/T_f$):[37] 33.3/55.7/59.4/61.8/69.1 (endotherm), 133.2/155.5/166.9/168.6/169.7 (endotherm) °C. TGA: onset of mass loss, 169 °C. Anal. Calcd (%) for $C_{54}H_{108}Cl_2P_2Pt$ (1085.37): C, 59.76; H, 10.03. Found: C, 59.22; H, 9.64.

NMR ($CDCl_3$, δ/ppm): ^1H (400 MHz) 2.10−1.85 (m, 12H, PCH_2), 1.64−1.49 (m, 12H, PCH_2CH_2), 1.48−1.40 (m, 12H, $PCH_2CH_2CH_2$), 1.40−1.18 (m, 72H, remaining CH_2); $^{13}C\{^1H\}$ (100 MHz)[39] 30.9 (virtual t,[41] $^3J_{CP}$ = 6.8 Hz, $PCH_2CH_2CH_2$), 28.9 (s, $2CH_2$), 28.6 (s, CH_2), 28.0 (s, CH_2), 27.3 (s, CH_2), 27.1 (s, CH_2), 26.5 (s, PCH_2CH_2), 24.6 (br s, PCH_2); $^{31}P\{^1H\}$ (162 MHz) 4.6 (s, $^1J_{PPt}$ = 3533 Hz[42]). MS:[43] 1084 (M^+, 15%), 1049 ($[M - Cl]^+$, 80%), 1011 (unassigned, 100%).

*4.1.8. cis-$PtCl_2(P((CH_2)_{20})_3P)$ (cis-**2f**).* Grubbs' first generation catalyst (0.0298 g, 0.0362 mmol, 7.5 mol %), *cis*-**1f** (0.6001 g, 0.481 mmol), and CH_2Cl_2 (450 mL; the resulting solution is 0.0011 M in *cis*-**1f**) were combined in a procedure analogous to that for the metathesis of *cis*-**1b**. After the alumina filtration step, the CH_2Cl_2 filtrate, PtO_2 (0.0232 g, 0.102 mmol), and H_2 (5 bar) were combined in a Fischer−Porter bottle. A reaction and workup analogous to that for *cis*-**2b** gave *cis*-**2f** (0.1017 g, 0.087 mmol, 18%) as a white solid, mp (capillary) 163−167 °C. Anal. Calcd (%) for $C_{60}H_{120}P_2Cl_2Pt$ (1169.53): C, 61.62; H, 10.34. Found C, 61.40; H, 10.29.

NMR ($CDCl_3$, δ/ppm): ^1H (500 MHz) 2.08−1.85 (m, 12H, PCH_2), 1.60−1.50 (m, 12H, PCH_2CH_2), 1.45−1.37 (m, 12H, $PCH_2CH_2CH_2$), 1.36−1.17 (m, 84H, remaining CH_2); $^{13}C\{^1H\}$ (126 MHz)[39] 31.2 (virtual t,[41] J_{CP} = 6.9 Hz, $PCH_2CH_2CH_2$), 29.4 (s, CH_2), 29.2 (s, CH_2), 28.9 (s, CH_2), 28.4 (s, CH_2), 27.9 (s, CH_2), 27.2 (s, CH_2), 27.1 (s, CH_2), 24.9 (br s, PCH_2CH_2), 24.6 (br s, PCH_2); $^{31}P\{^1H\}$ (202 MHz) 2.84 (s, $^1J_{PPt}$ = 3540 Hz[42]). IR (cm^{-1}, powder film): 2916 (s), 2847 (m), 1458 (m), 718 (m).

*4.1.9. cis-$PtCl_2(P((CH_2)_{22})_3P)$ (cis-**2g**).* Grubbs' first generation catalyst (0.0254 g, 0.0309 mmol, 9.4 mol %), *cis*-**1g** (0.4382 g, 0.329 mmol), and CH_2Cl_2 (450 mL; the resulting solution is 0.00073 M in *cis*-**1g**) were combined in a procedure analogous to that for the metathesis of *cis*-**1b**. After the alumina filtration step, the CH_2Cl_2 filtrate (20 mL), PtO_2 (0.0185 g, 0.0815 mmol), and H_2 (5 bar) were combined in a Fischer−Porter bottle. A reaction and workup analogous to that for *cis*-**2b** gave *cis*-**2g** (0.0871 g, 0.0695 mmol, 21%) as a white solid, mp (capillary) 134−137 °C. Anal. Calcd (%) for $C_{66}H_{132}P_2Cl_2Pt$ (1253.69): C, 63.23; H, 10.61. Found C, 63.50; H, 10.73.

NMR ($CDCl_3$, δ/ppm): ^1H (500 MHz) 2.08−1.85 (m, 12H, PCH_2), 1.62−1.50 (m, 12H, PCH_2CH_2), 1.44−1.37 (m, 12H, $PCH_2CH_2CH_2$), 1.36−1.20 (m, 96H, remaining CH_2); $^{13}C\{^1H\}$ (126 MHz)[39] 31.1 (virtual t,[41] J_{CP} = 7.1 Hz, $PCH_2CH_2CH_2$), 29.4 (s, $2CH_2$), 29.3 (s, CH_2), 28.9 (s, CH_2), 28.4 (s, CH_2), 27.9 (s, CH_2), 27.7 (s, CH_2), 27.3 (s, CH_2), 24.7 (apparent br m, PCH_2CH_2); $^{31}P\{^1H\}$ (202 MHz) 2.27 (s, $^1J_{PPt}$ = 3530 Hz[42]). IR (cm^{-1}, powder film): 2916 (s), 2846 (m), 1458 (m), 718 (m).

*4.1.10. cis-$PtCl_2(P(O(CH_2)_3CH{=}CH_2)_3)_2$ (cis-**4a**).* A Schlenk flask was charged with $PtCl_2$ (0.250 g, 0.940 mmol), toluene (10.0 mL), and $P(O(CH_2)_3CH{=}CH_2)_3$ (0.5920 g, 2.068 mmol).[24] The mixture was refluxed with stirring (12 h). The solvent was removed by oil pump vacuum, and CH_2Cl_2 was added. The sample was chromatographed (silica column, 70:30 v/v hexanes/ethyl acetate). The solvent was removed from the product containing fractions by oil pump vacuum to give *cis*-**4a** (0.474 g, 0.565 mmol, 60%) as a light yellow oil. Anal. Calcd (%) for $C_{30}H_{54}Cl_2O_6P_2Pt$ (838.68): C, 42.96; H, 6.49. Found: C, 43.57; H, 6.73.[38]

NMR ($CDCl_3$, δ/ppm): ^1H (400 MHz) 5.78 (ddt, 6H, $^3J_{HHtrans}$ = 17.1 Hz, $^3J_{HHcis}$ = 10.3 Hz, $^3J_{HH}$ = 6.6 Hz, $CH{=}$), 5.02 (dd, 6H, $^3J_{HHtrans}$ = 17.9 Hz, $^2J_{HH}$ = 1.6 Hz, $={CH_EH_Z}$), 4.99 (br d, 6H, $^3J_{HHcis}$ = 10.2 Hz, $={CH_EH_Z}$), 4.18−4.93 (m, 12H, OCH_2), 2.16−2.11 (m, 12H, CH_2), 1.81−1.74 (m, 12H, CH_2); $^{13}C\{^1H\}$ (100 MHz) 137.6 (s, $CH{=}$), 115.9 (s, $={CH_2}$), 67.3 (s, OCH_2), 30.0 (s, $CH_2CH{=}$), 29.7 (virtual t,[41] J_{CP} = 3.6 Hz, OCH_2CH_2); $^{31}P\{^1H\}$ (162 MHz) 69.7 (s, $^1J_{PPt}$ = 5696 Hz[42]). MS:[43] 803 ($M^+ - Cl$, 40%), 767 ($M^+ - 2Cl$, 8%), 343 (unassigned, 100%).

*4.1.11. cis-$PtCl_2(P(O(CH_2)_4CH{=}CH_2)_3)_2$ (cis-**4b**).* $PtCl_2$ (0.100 g, 0.376 mmol), toluene (5.5 mL), and $P(O(CH_2)_4CH{=}CH_2)_3$ (0.272 g, 0.827 mmol)[24] were combined in a procedure analogous to that for *cis*-**4a**. An identical workup gave *cis*-**4b** (0.2275 g, 0.2465 mmol, 66%) as a colorless oil. Anal. Calcd (%) for $C_{36}H_{66}Cl_2O_6P_2Pt$ (922.84): C, 46.86; H, 7.21. Found: C, 46.94; H, 7.46.

NMR ($CDCl_3$, δ/ppm): ^1H (400 MHz) 5.76 (ddt, 6H, $^3J_{HHtrans}$ = 17.0 Hz, $^3J_{HHcis}$ = 10.2 Hz, $^3J_{HH}$ = 6.6 Hz, $CH{=}$), 4.99 (br d, 6H, $^3J_{HHtrans}$ = 17.6 Hz, $={CH_EH_Z}$), 4.96 (br d, 6H, $^3J_{HHcis}$ = 10.3 Hz, $={CH_EH_Z}$), 4.16−4.12 (m, 12H, OCH_2), 2.09−2.02 (m, 12H, CH_2), 1.71−1.64 (m, 12H, CH_2), 1.49−1.42 (m, 12H, remaining CH_2); $^{13}C\{^1H\}$ (100 MHz) 138.5 (s, $CH{=}$), 115.4 (s, $={CH_2}$), 67.7 (s, OCH_2), 33.6 (s, CH_2), 30.0 (s, CH_2), 25.2 (s, CH_2); $^{31}P\{^1H\}$ (162 MHz) 69.3 (s, $^1J_{PPt}$ = 5696 Hz[42]). MS:[43] 887 ($M^+ - Cl$, 25%), 850 ($M^+ - 2Cl$, < 5%), 357 (100%).

*4.1.12. cis-$PtCl_2(P(O(CH_2)_5CH{=}CH_2)_3)_2$ (cis-**4c**).* $PtCl_2$ (0.250 g, 0.940 mmol), toluene (10.0 mL), and $P(O(CH_2)_5CH{=}CH_2)_3$ (0.766 g, 2.068 mmol)[24] were combined in a procedure analogous to that for *cis*-**4a**.

DOI: 10.1021/jacs.8b02846
J. Am. Chem. Soc. 2018, 140, 8463−8478

An identical workup gave *cis*-**4c** (0.900 g, 0.894 mmol, 95%) as colorless oil. Anal. Calcd (%) for $C_{42}H_{78}Cl_2O_6P_2Pt$ (1007.00): C, 50.10; H, 7.81. Found: C, 49.78; H, 7.81.

NMR ($CDCl_3$, δ/ppm): ^{1}H (400 MHz) 5.77 (ddt, 6H, $^3J_{HHtrans}$ = 17.1 Hz, $^3J_{HHcis}$ = 10.3 Hz, $^3J_{HH}$ = 6.7 Hz, C*H*═), 4.98 (dd, 6H, $^3J_{HHtrans}$ = 17.2 Hz, $^2J_{HH}$ = 1.7 Hz, ═CH$_E$*H*$_Z$), 4.93 (br d, 6H, $^3J_{HHcis}$ = 10.2 Hz, ═C*H*$_E$H$_Z$), 4.15−4.07 (m, 12H, OC*H*$_2$), 2.06−2.01 (m, 12H, C*H*$_2$), 1.70−1.64 (m, 12H, C*H*$_2$), 1.39−1.35 (m, 24H, remaining C*H*$_2$); ^{13}C{^{1}H} (100 MHz) 138.9 (s, *C*H═), 115.1 (s, ═*C*H$_2$), 67.7 (s, OCH$_2$), 34.0 (s, CH$_2$), 30.1 (s, CH$_2$), 28.9 (s, CH$_2$), 25.5 (s, CH$_2$); ^{31}P{^{1}H} (162 MHz) 69.3 (s, $^1J_{PPt}$ = 5698 Hz[42]). MS:[43] 971 (M^+ − Cl, 100%), 371 ([P(O(CH$_2$)$_5$CH═CH$_2$)$_3$]$^+$, 100%).

*4.1.13. Metathesis of cis-**4a**.* A Schlenk flask was charged with *cis*-**4a** (0.166 g, 0.198 mmol), Grubbs' first generation catalyst (0.0163 g, 0.0198 mmol, 10 mol %), and CH_2Cl_2 (250 mL; the resulting solution is 0.00079 M in *cis*-**4a**) and fitted with a condenser. The solution was refluxed with stirring (12 h). The mixture was cooled to room temperature, and a second charge of Grubbs' first generation catalyst (0.008 g, 0.009 mmol, 5 mol %) was added. The solution was refluxed with stirring (12 h). A third cycle with 5 mol % of Grubbs' first generation catalyst was similarly conducted. The solvent was removed by oil pump vacuum, and CH_2Cl_2 (2 mL) was added. The mixture was chromatographed (silica column, 80:20 v/v hexanes/ethyl acetate). A yellow band and then a colorless product band were collected. The solvent was removed from the latter by oil pump vacuum, and ethyl ether was added. The ether was removed by oil pump vacuum, and the cycle repeated until metathesized *cis*-**4a** (0.0450 g, 0.0596 mmol, 30%) was obtained as a white solid.

NMR ($CDCl_3$, δ/ppm): ^{1}H (400 MHz) 5.49−5.04 (m, 6H, C*H*═), 4.51−4.02 (m, 12H, OC*H*$_2$), 2.41−1.52 (m, 24H, remaining C*H*$_2$); ^{31}P{^{1}H} (162 MHz) 76.0 (s, 23%), 72.9 (s, 37%), 69.1 (s, 23%), 68.7 (s, 17%).

*4.1.14. cis-PtCl$_2$(P(O(CH$_2$)$_8$O)$_3$P) (cis-**5a**).* A Fischer−Porter bottle was charged with metathesized *cis*-**4a** (0.045 g, 0.060 mmol), $(Ph_3P)_3RhCl$ (0.0110 g, 0.0119 mmol, 20 mol %), toluene (20 mL), and H_2 (5 bar). The solution was stirred at 70 °C (12 h). The solvent was removed by oil pump vacuum. The mixture was chromatographed (silica column, 80:20 v/v hexanes/ethyl acetate). A yellow band and then a colorless product band were collected. The solvent was removed from the latter by oil pump vacuum. Ethyl ether was added and then removed by oil pump vacuum; hexanes were added and then removed by oil pump vacuum. This cycle was repeated until *cis*-**5a** (0.015 g, 0.020 mmol, 33%) was obtained as a white solid, mp (capillary) 195 °C. DSC (T_i/T_e/T_p/T_c/T_f):[37] 85.8/111.0/123.6/130.4/141.4 °C (endotherm). TGA: onset of mass loss, 289 °C. Anal. Calcd (%) for $C_{24}H_{48}Cl_2O_6P_2Pt$ (760.57): C, 37.90; H, 6.36. Found: C, 38.45; H, 6.27.[38]

NMR ($CDCl_3$, δ/ppm): ^{1}H (400 MHz) 5.00−4.95 (m, 4H, OC*H*$_2$), 4.21−4.19 (m, 4H, OC*H*$_2$), 4.09−3.94 (m, 4H, OC*H*$_2$), 2.02−1.92 (m, 4H, C*H*$_2$), 1.80−1.74 (m, 4H, C*H*$_2$), 1.62−1.54 (m, 16H, C*H*$_2$), 1.40−1.21 (m, 12H, remaining C*H*$_2$); ^{13}C{^{1}H} (100 MHz) 69.0 (s, 4C, OCH$_2$), 65.4 (virtual t,[41] J_{CP} = 4.6 Hz, 2C, OCH$_2$), 29.0 (s, 4C, CH$_2$), 28.1 (s, 2C, CH$_2$), 26.5 (s, 4C, CH$_2$), 24.0 (s, 4C, CH$_2$), 23.9 (s, 2C, CH$_2$), 20.8 (s, 2C, CH$_2$); ^{31}P{^{1}H} (162 MHz) 68.2 (s, $^1J_{PPt}$ = 5729 Hz[42]). MS:[43] 759 (M^+, 20%), 723 (M^+ − Cl, 60%), 687 (M^+ − 2Cl, 100%).

*4.1.15. Metathesis of cis-**4b**.* Grubbs' first generation catalyst (0.010 g, 0.012 mmol, 10 mol %), *cis*-**4b** (0.113 g, 0.122 mmol), and CH_2Cl_2 (125 mL; the resulting solution is 0.00098 M in *cis*-**4b**) were combined in a procedure analogous to that for the metathesis of *cis*-**4a**. An identical workup gave metathesized *cis*-**4b** (0.046 g, 0.055 mmol, 45%) as a white solid.

NMR ($CDCl_3$, δ/ppm): ^{1}H (400 MHz) 5.41−5.31 (m, 6H, C*H*═), 4.54−4.43 (m, 4H, OC*H*$_2$), 3.92−3.88 (m, 8H, OC*H*$_2$), 2.09−1.17 (m, 36H, remaining C*H*$_2$); ^{31}P{^{1}H} (162 MHz) 68.2 (s, 22%), 68.00 (s, 46%), 67.96 (13%), 67.8 (s, 19%).

*4.1.16. cis-PtCl$_2$(P(O(CH$_2$)$_{10}$O)$_3$P) (cis-**5b**).* Metathesized *cis*-**4b** (0.039 g, 0.046 mmol), $(Ph_3P)_3RhCl$ (0.0064 g, 0.0069 mmol, 15 mol %), toluene (20 mL), and H_2 (5 bar) were combined in a procedure analogous to that for *cis*-**5a**. An identical workup gave *cis*-**5b** (0.017 g, 0.020 mmol, 44%) as a white solid, mp (capillary) 146 °C. DSC (T_i/T_e/T_p/T_c/T_f):[37] 51.2/61.4/72.1/83.8/88.0 (endotherm), 116.3/142.7/146.2/147.6/155.1 °C (endotherm). TGA: onset of mass loss, 276 °C. Anal. Calcd (%) for $C_{30}H_{60}Cl_2O_6P_2Pt$ (844.73): C, 42.66; H, 7.16. Found: C, 42.96; H, 7.53.

NMR ($CDCl_3$, δ/ppm): ^{1}H (400 MHz) 4.58−4.52 (m, 4H, OC*H*$_2$), 4.13−4.04 (m, 4H, OC*H*$_2$), 4.00−3.96 (m, 4H, OC*H*$_2$), 1.81−1.68 (m, 12H, OCH$_2$C*H*$_2$), 1.48−1.34 (m, 36H, remaining C*H*$_2$); ^{13}C{^{1}H} (100 MHz) 68.5 (s, 4C, OCH$_2$), 65.7 (br s, 2C, OCH$_2$), 29.1 (s, 4C, CH$_2$), 28.5 (s, 2C, CH$_2$), 26.9 (s, 4C, CH$_2$), 26.8 (2s, 6C, CH$_2$), 24.8 (s, 2C, CH$_2$), 23.9 (s, 4C, CH$_2$), 22.9 (s, 2C, CH$_2$); ^{31}P{^{1}H} (162 MHz) 68.1 (s, $^1J_{PPt}$ = 5759 Hz[42]). MS:[43] 810 (M^+ − Cl, 100%), 772 (M^+ − 2Cl, 40%).

*4.1.17. Metathesis of cis-**4c**.* Grubbs' first generation catalyst (0.024 g, 0.030 mmol, 10 mol %), *cis*-**4c** (0.300 g, 0.298 mmol), and CH_2Cl_2 (300 mL; the resulting solution is 0.00099 M in *cis*-**4c**) were combined in a procedure analogous to that for the metathesis of *cis*-**4a**. An identical workup gave metathesized *cis*-**4c** (0.150 g, 0.163 mmol, 55%) as colorless foam.

NMR ($CDCl_3$, δ/ppm): ^{1}H (400 MHz) 5.38−5.23 (m, 6H, CH═), 4.45−4.39 (m, 4H, OCH$_2$), 4.21−4.07 (m, 8H, OCH$_2$), 2.26−2.06 (m, 12H, CH$_2$), 1.89−1.39 (m, 36H, remaining C*H*$_2$); ^{31}P{^{1}H} (162 MHz) 67.4 (s).

*4.1.18. cis-PtCl$_2$(P(O(CH$_2$)$_{12}$O)$_3$P) (cis-**5c**).* Metathesized *cis*-**4c** (0.0440 g, 0.0477 mmol), $(Ph_3P)_3RhCl$ (0.0083 g, 0.0095 mmol, 20 mol %), toluene (20 mL), and H_2 (5 bar) were combined in a procedure analogous to that for *cis*-**5a**. An identical workup gave *cis*-**5c** (0.016 g, 0.017 mmol, 36%) as white foam. Anal. Calcd (%) for $C_{36}H_{72}Cl_2O_6P_2Pt$ (928.89): C, 46.55; H, 7.81. Found: C, 47.23; H, 7.97.[38]

NMR ($CDCl_3$, δ/ppm): ^{1}H (400 MHz) 4.33−4.30 (m, 4H, OC*H*$_2$), 4.17−4.14 (m, 8H, OC*H*$_2$), 1.75−1.58 (m, 12H, C*H*$_2$), 1.42−1.34 (m, 48H, remaining C*H*$_2$; ^{13}C{^{1}H} (100 MHz) 68.0 (s, 4C, OCH$_2$), 67.8 (virtual t,[41] J_{CP} = 2.6 Hz, 2C, OCH$_2$), 30.1 (virtual t,[41] J_{CP} = 3.1 Hz, 2C, CH$_2$), 29.7 (virtual t,[41] J_{CP} = 3.1 Hz, 4C, CH$_2$), 27.3 (s, 2C, CH$_2$), 27.1 (s, 2C, CH$_2$), 26.8 (s, 4C, CH$_2$), 26.7 (s, 4C, CH$_2$), 26.3 (s, 2C, CH$_2$), 26.1 (s, 4C, CH$_2$), 24.7 (s, 2C, CH$_2$), 24.3 (s, 4C, CH$_2$); ^{31}P{^{1}H} (162 MHz) 68.3 (s, $^1J_{PPt}$ = 5721 Hz[42]). MS:[43] 894 (M^+ − Cl, 100%), 856 (M^+ − 2Cl, 45%).

*4.1.19. cis-PtPh$_2$(P((CH$_2$)$_{14}$)$_3$P) (cis-**6c**).* A Schlenk flask was charged with *cis*-**2c** (0.0502 g, 0.0545 mmol) and Ph_2Zn (0.0375 g, 0.171 mmol), and THF (5 mL) was added with stirring. After 18 h, CH_3OH (several drops) was added. The sample was exposed to air. After 1 h, the solvent was removed by oil pump vacuum, and benzene was added. The suspension was filtered through a pipet filled with silica, which was rinsed with benzene. The solvent was removed from the combined filtrate by oil pump vacuum to give *cis*-**6c** (0.0381 g, 0.0379 mol, 70%) as a white solid, dec pt. (capillary) 160 °C. Anal. Calcd (%) for $C_{54}H_{94}P_2Pt$ (1000.36): C, 64.84; H, 9.47. Found: C, 61.87; H, 9.42.[38]

NMR ($CDCl_3$, δ/ppm): ^{1}H (400 MHz) 7.34 (m, 4H, *o*-Ph),[44] 6.83 (t, $^3J_{HH}$ = 6.9 Hz, 4H, *m*-Ph), 6.63 (t, $^3J_{HH}$ = 6.8 Hz, 2H, *p*-Ph), 2.12−2.04 (m, 4H, PC*H*$_2$), 1.90 (br, 4H, PC*H*$_2$), 1.47−1.24 (m, 4H/72H, PC*H*$_2$/remaining C*H*$_2$; ^{13}C{^{1}H} (100 MHz)[39,45] 136.4 (s, 4C, *o*-Ph), 126.8 (s, 4C, *m*-Ph), 120.7 (s, 2C, *p*-Ph), 30.8 (virtual t,[41] $^3J_{CP}$ = 4.3 Hz, 2C, PCH$_2$CH$_2$CH$_2$), 30.5 (virtual t,[41] $^3J_{CP}$ = 7.0 Hz, 4C, PCH$_2$CH$_2$CH$_2$), 28.5 (s, 6C, CH$_2$), 27.4 (s, 4C, CH$_2$), 27.3 (s, 4C, CH$_2$), 27.2 (s, 6C, CH$_2$), 27.0 (s, 6C, CH$_2$), 26.3 (s, 6C, PCH$_2$CH$_2$), 25.0 (s, 4C, PCH$_2$), 22.5 (br s, 2C, PCH$_2$); ^{31}P{^{1}H} (162 MHz) 1.0 (s, $^1J_{PPt}$ = 1779 Hz[42]). MS:[43] 920 (M^+ − C$_6$H$_5$, 25%), 844 (M^+ − 2C$_6$H$_5$, 100%).

*4.1.20. cis-PtPh$_2$(P((CH$_2$)$_{16}$)$_3$P) (cis-**6d**).* THF (5 mL), Ph_2Zn (0.0404 g, 0.184 mmol), and *cis*-**2d** (0.0621 g, 0.0620 mmol), were combined in a procedure analogous to that for *cis*-**6c**. An identical workup gave *cis*-**6d** (0.0458 g, 0.0422 mol, 68%) as a white solid, mp (capillary) 153 °C. Anal. Calcd (%) for $C_{60}H_{106}P_2Pt$ (1084.54): C, 66.45; H, 9.85. Found: C, 64.70; H, 10.01.[38]

NMR ($CDCl_3$, δ/ppm): ^{1}H (500 MHz) 7.33 (m, 4H, *o*-Ph),[44] 6.89 (t, $^3J_{HH}$ = 6.9 Hz, 4H, *m*-Ph), 6.68 (t, $^3J_{HH}$ = 6.8 Hz, 2H, *p*-Ph), 2.04−1.87 (m, 4H, PC*H*$_2$), 1.73 (br, 4H, PC*H*$_2$), 1.61−1.10 (m, 4H/84H,

DOI: 10.1021/jacs.8b02846
J. Am. Chem. Soc. 2018, 140, 8463−8478

PCH$_2$/remaining CH$_2$; ^{13}C{^{1}H} (126 MHz)[39,45] 136.4 (s, 4C, *o*-Ph), 126.7 (s, 4C, *m*-Ph), 120.6 (s, 2C, *p*-Ph), 31.3 (virtual t,[41] $^3J_{CP}$ = 4.3 Hz, 2C, PCH$_2$CH$_2$CH$_2$), 31.2 (virtual t,[41] $^3J_{CP}$ = 7.0 Hz, 4C, PCH$_2$CH$_2$CH$_2$), 29.2 (s, 4C, CH$_2$), 28.7 (s, 2C, CH$_2$), 28.33 (s, 2C, CH$_2$), 28.27 (s, 4C, CH$_2$), 27.9 (s, 4C, CH$_2$), 27.5 (s, 2C, CH$_2$), 27.0 (s, 2C, CH$_2$), 26.9 (s, 2C, CH$_2$), 26.8 (s, 4C, CH$_2$), 26.5 (s, 4C, CH$_2$), 25.4 (s, 6C, CH$_2$), 23.6 (s, 4C, PCH$_2$), 22.5 (br s, 2C, PCH$_2$); ^{31}P{^{1}H} (202 MHz) −0.68 (s, $^1J_{PPt}$ = 1778 Hz[42]). IR (cm^{-1}, powder film): 3043 (w), 2920 (s), 2850 (m), 1568 (w), 1458 (m), 1261 (m), 1091 (m), 1055 (m), 1020 (m), 800 (m).

*4.1.21. cis-PtI$_2$(P(O(CH$_2$)$_{10}$O)$_3$P) (cis-**7b**).* An NMR tube was charged with *cis*-**5b** (0.0101 g, 0.0118 mmol), NaI (0.0071g, 0.047 mmol), and THF/acetone (0.6 mL, 50:50 v/v). After 17 h, a ^{31}P{^{1}H} NMR spectrum showed >99% conversion. The solvent was removed by oil pump vacuum, and benzene was added. The suspension was filtered through glass fibers. The solvent was removed from the filtrate by oil pump vacuum to give a yellow oil. Hexanes were added and then removed by oil pump vacuum. Pentane was added and then removed by oil pump vacuum to give *cis*-**7b** (0.0119 g, 0.0116 mmol, 98%) as a yellow solid, mp (capillary) 147 °C. Anal. Calcd (%) for C$_{30}$H$_{60}$I$_2$O$_6$P$_2$Pt (1027.63): C, 35.06; H, 5.88. Found: C, 37.56; H, 6.24.[38]

NMR (CDCl$_3$, δ/ppm): ^{1}H (400 MHz) 4.47−4.38 (m, 4H, OCH$_2$), 4.15−4.07 (m, 4H, OCH$_2$), 3.99−3.94 (m, 4H, OCH$_2$), 1.84−1.71 (m, 12H, OCH$_2$CH$_2$), 1.40−1.23 (m, 36H, remaining CH$_2$); ^{13}C{^{1}H} (100 MHz) 69.4 (s, 4C, OCH$_2$), 66.2 (d, $^2J_{CP}$ = 9.8 Hz, 2C, OCH$_2$), 29.2 (d, 4C, $^3J_{CP}$ = 5.8 Hz OCH$_2$CH$_2$), 28.6 (d, 2C, $^3J_{CP}$ = 7.7 Hz, OCH$_2$CH$_2$), 27.25 (s, 4C, CH$_2$), 27.22 (s, 4C, CH$_2$), 25.3 (s, 2C, CH$_2$), 25.1 (s, 2C, CH$_2$), 24.2 (s, 4C, CH$_2$), 23.3 (s, 2C, CH$_2$); ^{31}P{^{1}H} (162 MHz) 72.6 (s, $^1J_{PPt}$ = 5517 Hz[42]). MS:[43] 901 (M$^+$ − I, 100%), 772 (M$^+$ − 2I, 50%).

*4.1.22. fac-ReCl(CO)$_3$(P((CH$_2$)$_6$CH=CH$_2$)$_3$)$_2$ (fac-**10c**).* A Schlenk flask was charged with ReCl(CO)$_5$ (0.500 g, 1.38 mmol),[46] THF (15 mL), and P((CH$_2$)$_6$CH=CH$_2$)$_3$ (1.011 g, 2.773 mmol)[14] and fitted with a condenser. The yellow solution was stirred at 60 °C and turned orange as gas evolved. After 21 h, the solution was cooled, and the solvent was removed by rotary evaporation and oil pump vacuum. The residue was chromatographed (alumina column, 3 cm × 15 cm; 4:1 and then 2:1 v/v hexanes/CH$_2$Cl$_2$). The solvent was removed from the major yellow band by oil pump vacuum to give *fac*-**10c** (0.953 g, 0.921 mmol, 67%) as a colorless viscous oil. Anal. Calcd (%) for C$_{51}$H$_{90}$ClO$_3$P$_2$Re (1034.87): C, 59.19; H, 8.77. Found C, 59.05; H, 8.76.

NMR (C$_6$D$_6$, δ/ppm):[47] ^{1}H (300 MHz) 5.78 (ddt, 6H, $^3J_{HHtrans}$ = 16.8 Hz, $^3J_{HHcis}$ = 10.2 Hz, $^3J_{HH}$ = 6.6 Hz, CH=), 5.05 (br d, $^3J_{HHtrans}$ = 17.3 Hz, 6H, =CH$_E$H$_Z$), 5.00 (br d, $^3J_{HHcis}$ = 11.1 Hz, 6H, =CH$_E$H$_Z$), 2.14−1.82 (br m, 12H/12H, CH$_2$CH=CH$_2$/PCH$_2$), 1.72−1.50 (br m, 12H, PCH$_2$CH$_2$), 1.42−1.22 (br m, 36H, remaining CH$_2$); ^{13}C{^{1}H} (100 MHz) 192.3/192.1/191.8/191.6/191.3 (apparent s/s/s/s/m, unassigned $^2J_{CP}$, 3CO), 138.9 (s, CH=), 114.7 (s, =CH$_2$), 34.0 (s, CH$_2$), 31.5 (virtual t,[41] $^3J_{CP}$ = 6.0 Hz, PCH$_2$CH$_2$CH$_2$), 29.11 (s, CH$_2$), 29.06 (s, CH$_2$), 26.5 (virtual t,[41] $^1J_{CP}$ = 12.9 Hz, PCH$_2$), 24.0 (s, PCH$_2$CH$_2$); ^{31}P{^{1}H} (121 MHz) −16.6 (s). IR (cm^{-1}, oil film): 2019 (s, ν_{CO}), 1930 (s, ν_{CO}), 1884 (s, ν_{CO}), 1640 (m, $\nu_{C=C}$). MS:[43] 1034[48] (M$^+$, 5%), 1007 (M$^+$ − CO, 45%), 1000 (M$^+$ − Cl, 100%).

*4.1.23. fac-ReBr(CO)$_3$(P((CH$_2$)$_6$CH=CH$_2$)$_3$)$_2$ (fac-**11c**).* THF (15 mL), ReBr(CO)$_5$ (0.500 g, 1.23 mmol),[46] and P((CH$_2$)$_6$CH=CH$_2$)$_3$ (0.912 g, 2.50 mmol)[14] were combined in a procedure analogous to that for *fac*-**10c**, except that the solution was stirred at 80 °C. A similar workup (alumina column, 3 cm × 15 cm; hexanes and then 4:1 v/v hexanes/CH$_2$Cl$_2$) gave *fac*-**11c** (0.575 g, 0.533 mmol, 43%) as a yellow viscous oil. Anal. Calcd (%) for C$_{51}$H$_{90}$BrO$_3$P$_2$Re (1079.31): C, 56.75; H, 8.40. Found C, 56.28; H 8.53.

NMR (C$_6$D$_6$, δ/ppm):[47] ^{1}H (300 MHz) 5.78 (ddt, 6H, $^3J_{HHtrans}$ = 16.8 Hz, $^3J_{HHcis}$ = 10.2 Hz, $^3J_{HH}$ = 6.6 Hz, CH=), 5.05 (br d, $^3J_{HHtrans}$ = 16.6 Hz, 6H, =CH$_E$H$_Z$), 5.00 (br d, $^3J_{HHcis}$ = 11.1 Hz, 6H, =CH$_E$H$_Z$), 2.12−1.80 (br m, 12H/12H, CH$_2$CH=CH$_2$/PCH$_2$), 1.67−1.47 (br m, 12H, PCH$_2$CH$_2$), 1.40−1.18 (br m, 36H, remaining CH$_2$); ^{13}C{^{1}H} (75 MHz) 191.5/191.2/190.9/190.6/190.3 (apparent s/s/s/m/s, unassigned $^2J_{CP}$, 3CO), 138.9 (s, CH=), 114.8 (s, =CH$_2$), 34.1 (s, CH$_2$), 31.4 (virtual t,[41] $^3J_{CP}$ = 5.8 Hz, PCH$_2$CH$_2$CH$_2$), 29.10 (s, CH$_2$), 29.08 (s, CH$_2$), 27.0 (virtual t,[41] $^1J_{CP}$ = 13.3 Hz, PCH$_2$), 24.2 (s, PCH$_2$CH$_2$); ^{31}P{^{1}H} (121 MHz) −22.4 (s). IR (cm^{-1}, oil film): 2023 (s, ν_{CO}), 1934 (s, ν_{CO}), 1888 (s, ν_{CO}), 1640 (m, $\nu_{C=C}$). MS:[43] 1078[49] (M$^+$, 8%), 1050[49] (M$^+$ − CO, 50%), 999[49] (M$^+$ − Br, 100%).

*4.1.24. Metathesis of fac-**10c**.* A three necked flask was charged with *fac*-**10c** (0.795 g, 0.768 mmol) and C$_6$H$_5$Cl (700 mL; the resulting solution is 0.0011 M in *fac*-**10c**) and fitted with a condenser. Grubbs' first generation catalyst (0.031 g, 0.038 mmol, 5 mol %) was added. Then N$_2$ was sparged through the solution with stirring. After 1 d, the solution was filtered through alumina, which was rinsed with CH$_2$Cl$_2$. The solvent was removed from the combined filtrates by oil pump vacuum to give metathesized *fac*-**10c** (0.558 g, 0.587 mmol, 76%) as a yellow viscous oil.

NMR (C$_6$D$_6$, δ/ppm): ^{1}H (300 MHz) 5.67−5.20 (br m, 6H, CH=), 2.45−1.86 (br m, 12H, CH$_2$CH=CH), 1.84−1.60 (br m, 12H, PCH$_2$), 1.59−1.16 (br m, 60H, remaining CH$_2$); ^{31}P{^{1}H} (121 MHz) −14.7 (s, 10%), −15.1 (s, 26%), −15.3 (s, 39%), −15.5 (s, 25%). MS:[43] 1846[50] (2M$^+$ − 2CO, 15%), 1836[50] (2M$^+$ − CO − Cl, 50%), 1815[50] (2M$^+$ − 3CO, 100%), 1786[50] (2M$^+$ − 4CO, 25%), 1774[50] (2M$^+$ − 2CO − 2Cl, 30%), 1747[50] (2M$^+$ − 3CO − 2Cl, 5%), 922 (M$^+$ − CO, 5%), 894 (M$^+$ − 2CO, 5%).

*4.1.25. Metathesis of fac-**11c**.* Grubbs' first generation catalyst (0.017 g, 0.021 mmol, 5 mol %), *fac*-**11c** (0.450 g, 0.417 mmol), and C$_6$H$_5$Cl (400 mL; the resulting solution is 0.0010 M in *fac*-**11c**) were combined in a procedure analogous to that for the metathesis of *fac*-**10c**. An identical workup gave metathesized *fac*-**11c** (0.329 g, 0.331 mmol, 79%) as a yellow viscous oil.

NMR (C$_6$D$_6$, δ/ppm): ^{1}H (300 MHz) 5.60−5.18 (br m, 6H, CH=), 2.31−1.87 (br m, 12H/12H, CH$_2$CH=CH/PCH$_2$), 1.80−1.01 (br m, 48H, remaining CH$_2$); ^{31}P{^{1}H} (121 MHz) −20.3 (s, 22%), −21.0 (s, 29%), −21.1 (s, 29%), −21.3 (s, 20%). MS:[43] 995[51] (M$^+$, 35%), 967[52] (M$^+$ − CO, 100%), 916 (M$^+$ − Br, 95%).

*4.1.26. fac-ReCl(CO)$_3$(P(CH$_2$)$_{13}$CH$_2$)((CH$_2$)$_{14}$)(P(CH$_2$)$_{13}$CH$_2$) (fac-**12′c**).* A Schlenk flask was charged with metathesized *fac*-**10c** (0.558 g, 0.587 mmol; the entire quantity prepared above), THF (10 mL), and PtO$_2$ (0.013 g, 0.057 mmol), connected to a balloon, and partially evacuated. Then H$_2$ was introduced (1 bar), and the suspension was stirred. After 1 d, the solvent was removed by oil pump vacuum. The residue was chromatographed (alumina column, 3 cm × 20 cm, 1:1 v/v hexanes/CH$_2$Cl$_2$). The solvent was removed from the product containing fractions by rotary evaporation and oil pump vacuum to give *fac*-**12′c** (0.283 g, 0.296 mmol, 50%; 39% from *fac*-**10c**) as a white solid, mp (capillary) 76 °C, DSC (T_i/T_e/T_p/T_c/T_f):[37] 36.57/36.87/41.14/45.42/46.10 °C (endotherm); 146.37/167.04/186.96/205.24/220.99 °C (exotherm). TGA: onset of mass loss, 279 °C. Anal. Calcd (%) for C$_{45}$H$_{84}$ClO$_3$P$_2$Re (956.75): C, 56.49; H 8.85. Found C, 56.21; H 8.50.

NMR (C$_6$D$_6$, δ/ppm):[47] ^{1}H (300 MHz) 2.29−1.89 (br m, 12H, PCH$_2$), 1.88−1.62 (br m, 12H, PCH$_2$CH$_2$), 1.60−1.18 (br m, 60H, remaining CH$_2$); ^{13}C{^{1}H} (75 MHz) 192.1/191.6/191.3 (apparent s/s/m, unassigned $^2J_{CP}$, 3CO), 31.2 (virtual t,[41] $^3J_{CP}$ = 6.4 Hz, PCH$_2$CH$_2$CH$_2$), 29.1 (virtual t,[41] $^3J_{CP}$ = 5.4 Hz, PCH$_2$CH$_2$CH$_2$), 27.6 (s, CH$_2$), 27.5 (virtual t,[41] $^1J_{CP}$ = 18.6 Hz, PCH$_2$),[53] 27.4 (s, CH$_2$), 27.1 (s, CH$_2$), 26.9 (virtual t,[41] $^1J_{CP}$ = 18.2 Hz, PCH$_2$),[53] 26.8 (s, CH$_2$), 26.2 (s, CH$_2$), 26.1 (s, CH$_2$), 26.0 (s, CH$_2$), 24.2 (s, CH$_2$), 22.6 (s, PCH$_2$CH$_2$), 22.4 (s, PCH$_2$CH$_2$); ^{31}P{^{1}H} (121 MHz) −15.7 (s). IR (cm^{-1}, powder film): 2019 (m, ν_{CO}), 1930 (s, ν_{CO}), 1880 (s, ν_{CO}). MS:[43] 957 (M$^+$, 30%), 929 (M$^+$ − CO, 70%), 922 (M$^+$ − Cl, 100%).

*4.1.27. fac-ReBr(CO)$_3$(P(CH$_2$)$_{13}$CH$_2$)((CH$_2$)$_{14}$)(P(CH$_2$)$_{13}$CH$_2$) (fac-**13′c**).* Metathesized *fac*-**11c** (0.329 g, 0.331 mmol; the entire quantity prepared above), THF (15 mL), and PtO$_2$ (0.020 g, 0.088 mmol) were combined in a procedure analogous to that for *fac*-**12′c**.[54] A similar workup (alumina column, 3 cm × 20 cm, 2:1 v/v hexanes/CH$_2$Cl$_2$) gave *fac*-**13′c** (0.062 g, 0.062 mmol, 19%; 15% from *fac*-**11c**) as a white solid, mp (capillary) 66 °C. DSC (T_i/T_e/T_p/T_c/T_f):[37] 146.26/170.84/191.10/241.88/242.08 °C (exotherm); 242.24/247.99/263.74/282.72/289.73 °C (exotherm, minor). TGA: onset of mass loss, 289 °C. Anal. Calcd (%) for C$_{45}$H$_{84}$BrO$_3$P$_2$Re (1001.21): C 53.98; H 8.46. Found C, 53.87; H 8.33.

NMR (C$_6$D$_6$, δ/ppm):[47] ^{1}H (300 MHz) 2.25−1.82 (br m, 12H, PCH$_2$), 1.80−1.59 (br m, 12H, PCH$_2$CH$_2$), 1.58−1.05 (br m, 60H,

DOI: 10.1021/jacs.8b02846
J. Am. Chem. Soc. 2018, 140, 8463−8478

remaining CH_2); $^{13}C\{^1H\}$ (100 MHz) 191.4/191.2/191.0/190.8/190.5 (apparent s/s/s/s/m, unassigned $^2J_{CP}$, 3CO), 31.1 (virtual t,[41] $^3J_{CP}$ = 6.4 Hz, $PCH_2CH_2CH_2$), 29.0 (br m, $PCH_2CH_2CH_2$), 27.6 (s, CH_2), 27.5 (virtual t,[41] $^1J_{CP}$ = 13.9 Hz, PCH_2),[53] 27.4 (s, CH_2), 27.1 (s, CH_2), 26.8 (d, $^3J_{CP}$ = 3.5 Hz, CH_2), 26.2 (s, CH_2), 26.1 (s, CH_2), 26.03 (s, CH_2), 25.95 (virtual t,[41] $^1J_{CP}$ = 13.9 Hz, PCH_2),[53] 24.3 (s, CH_2), 22.6 (s, PCH_2CH_2), 22.4 (s, PCH_2CH_2); $^{31}P\{^1H\}$ (121 MHz) −21.4 (s). IR (cm^{-1}, powder film): 2019 (m, ν_{CO}), 1934 (s, ν_{CO}), 1888 (s, ν_{CO}). MS:[43] 1001[52] (M^+, 15%), 972 (M^+ − CO, 70%), 944 (M^+ − 2CO, 35%), 921[49] (M^+ − Br, 100%).

4.2. Thermolyses of Platinum Complexes. The following are representative, and additional experiments are described in the SI. (A) An NMR tube was charged with *cis*-**2c** (0.0071 g, 0.0078 mmol) and *o*-$C_6H_4Cl_2$ (0.7 mL) and kept at 185 °C. The tube was periodically cooled, and $^{31}P\{^1H\}$ NMR spectra were recorded (Figure 9; δ/ppm: 6.46 (s, $^1J_{PPt}$ = 2395 Hz,[42] *trans*-**2c**), 4.04 (s, $^1J_{PPt}$ = 3540 Hz,[42] *cis*-**2c**)). The *trans*-**2c**/*cis*-**2c** ratios were 5:95 (1 d), 72:28 (3 d), 87:13 (4 d), 89:11 (5 d), and 89:11 (6 d). (B) An NMR tube was charged with *cis*-**2g** (0.0081 g, 0.0065 mmol) and C_6D_5Br (0.7 mL) and kept at 150 °C. The tube was periodically cooled, and $^{31}P\{^1H\}$ NMR spectra were recorded (Figure 10; δ/ppm: 5.32 (s, $^1J_{PPt}$ = 2388 Hz,[42] *trans*-**2g**), 3.21 (s, oligomer), 2.87 (s, $^1J_{PPt}$ = 3530 Hz,[42] *cis*-**2g**)). The *trans*-**2g**/*cis*-**2g**/oligomer ratios were 74:7:19 (1 d) and 65:6:29 (2 d). (C) An NMR tube was charged with *cis*-**2c** (0.0085 g, 0.0093 mmol) and C_6D_5Br (0.7 mL) and kept at 150 °C. The tube was periodically cooled, and $^{31}P\{^1H\}$ NMR spectra were recorded (Figure s5; δ/ppm: 7.21 (s, $^1J_{PPt}$ = 2395 Hz,[42] *trans*-**2c**), 5.25 (s, oligomer), 4.59 (s, $^1J_{PPt}$ = 3540 Hz,[42] *cis*-**2c**), 2.94 (s, $^1J_{PPt}$ = 2344 Hz,[42] *trans*-$PtBr_2(P((CH_2)_{14})_3P)$[4b,25]). The *trans*-**2g**/*cis*-**2g**/oligomer/*trans*-$PtBr_2(P((CH_2)_{14})_3P)$ ratios were 16:78:6:<1 (1 d), 22:62:16:<1 (2 d), and 22:<1:48:30 (3 d).

4.3. Thermolyses of Rhenium Complexes. The following is representative, and additional experiments are described in the SI. (A) A flask was charged with *fac*-**10c** (0.700 g, 0.649 mmol) and C_6H_5Cl (30 mL) and heated to 140 °C. The reaction was monitored by $^{31}P\{^1H\}$ NMR. After 21 h, conversion was complete. The solvent was removed by oil pump vacuum. The residue was chromatographed (alumina column, 3 × 20 cm, 1:1 v/v hexanes/CH_2Cl_2). The solvent was removed from the product-containing fractions by rotary evaporation and oil pump vacuum to give previously reported *mer*,*trans*-**11c** (0.625 g, 0.580 mmol, 89%)[6a] as a yellow viscous oil.

NMR (C_6D_6, δ/ppm): ^1H (300 MHz) 5.77 (ddt, $^3J_{HHtrans}$ = 16.9 Hz, $^3J_{HHcis}$ = 10.2 Hz, $^3J_{HH}$ = 6.7 Hz, 6H, CH═), 5.04 (br d, $^3J_{HHtrans}$ = 17.1 Hz, 6H, ═CH_EH_Z), 4.99 (br d, $^3J_{HHcis}$ = 10.3 Hz, 6H, ═CH_EH_Z), 2.11−2.00 (br m, 12H, CH_2CH═CH_2), 1.99−1.91 (br m, 12H, PCH_2), 1.69−1.51 (br m, 12H, PCH_2CH_2), 1.49−1.20 (br m, 36H, remaining CH_2); $^{31}P\{^1H\}$ (121 MHz) −13.2 (s). IR (cm^{-1}, oil film): 2026 (m, ν_{CO}), 1999 (m, ν_{CO}), 1934 (s, ν_{CO}), 1888 (s, ν_{CO}), 1640 (m, $\nu_{C=C}$).

■ ASSOCIATED CONTENT

Supporting Information

The Supporting Information is available free of charge on the ACS Publications website at DOI: 10.1021/jacs.8b02846.

Additional general, preparative, spectroscopic, and crystallographic data, calculations of $\Delta G^{\ddagger}$ values, and details of the DFT computations (PDF)

Molecular structure file that can be read by the program Mercury[55] and contains the optimized geometries of all computed structures[56] (XYZ)

Crystal structure of *cis*-**1f** (CIF)

Crystal structure of *cis*-**2c** (CIF)

Crystal structure of *cis*-**2d** (CIF)

Crystal structure of *cis*-**2f** (CIF)

Crystal structure of *cis*-**6c** (CIF)

Crystal structure of *cis*-**5a** (CIF)

Crystal structure of *cis*-**5b** (CIF)

■ AUTHOR INFORMATION

Corresponding Author

*gladysz@mail.chem.tamu.edu

ORCID

Hemant Joshi: 0000-0002-7616-0241

Sugam Kharel: 0000-0001-6106-4639

Andreas Ehnbom: 0000-0002-7044-1712

Tobias Fiedler: 0000-0001-7169-305X

John A. Gladysz: 0000-0002-7012-4872

Author Contributions

§H.J. and S.K. contributed equally to this work.

Notes

The authors declare no competing financial interest.

CCDC 1813023 (*cis*-**1f**), 1813021 (*cis*-**2c**), 1813024 (*cis*-**2d**), 1815513 (*cis*-**2f**), 693915 (*cis*-**5a**), 693916 (*cis*-**5b**), and 1813022 (*cis*-**6c**) contain the supplementary crystallographic data for this paper. These data can be obtained free of charge via www.ccdc.cam.ac.uk/data_request/cif, or by emailing data_request@ccdc.cam.ac.uk, or by contacting the Cambridge Crystallographic Data Centre, 12 Union Road, Cambridge CB2 1EZ, UK; fax: + 44 1123 336033.

■ ACKNOWLEDGMENTS

The authors thank the National Science Foundation (CHE-1153085, CHE-156601) and Deutsche Forschungsgemeinschaft (DFG, GL 300/9-1) for support, Dr. M. Barbasiewicz for useful observations, the Laboratory for Molecular Simulation and Texas A&M High Performance Research Computing for resources, and Prof. M. B. Hall and Dr. L. M. Pérez for helpful discussions.

■ REFERENCES

(1) Fiedler, T.; Gladysz, J. A. Multifold Ring Closing Olefin Metatheses in Syntheses of Organometallic Molecules with Unusual Connectivities. In *Olefin Metathesis − Theory and Practice*; Grela, K., Ed.; John Wiley & Sons: Hoboken, NJ, 2014; pp 311−328.

(2) Representative examples since the coverage in ref 1: (a) Wu, Q.; Rauscher, P. M.; Lang, X.; Wojtecki, R. J.; de Pablo, J. J.; Hore, M. J. A.; Rowan, S. J. *Science* **2017**, *358*, 1434−1439. (b) Danon, J. J.; Krüger, A.; Leigh, D. A.; Lemonnier, J.-F.; Stephens, A. J.; Vitorica-Yrezabal, I. J.; Woltering, S. L. *Science* **2017**, *355*, 159−162. (c) Ogasawara, M.; Tseng, Y.-Y.; Liu, Q.; Chang, N.; Yang, X.; Takahashi, T.; Kamikawa, K. *Organometallics* **2017**, *36*, 1430−1435 and earlier papers by this group cited therein. (d) Masuda, T.; Arase, J.; Inagaki, Y.; Kawahata, M.; Yamaguchi, K.; Ohhara, T.; Nakao, A.; Momma, H.; Kwon, E.; Setaka, W. *Cryst. Growth Des.* **2016**, *16*, 4392−4401 and earlier papers by this group cited therein. (e) Gil-Ramírez, G.; Hoekman, S.; Kitching, M. O.; Leigh, D. A.; Vitorica-Yrezabal, I. J.; Zhang, G. *J. Am. Chem. Soc.* **2016**, *138*, 13159−13162. (f) Cain, M. F.; Forrest, W. P., Jr.; Peryshkov, D. V.; Schrock, R. R.; Müller, P. *J. Am. Chem. Soc.* **2013**, *135*, 15338−15341.

(3) (a) Shima, T.; Hampel, F.; Gladysz, J. A. *Angew. Chem., Int. Ed.* **2004**, *43*, 5537−5540; *Angew. Chem.* **2004**, *116*, 5653−5656. (b) Lang, G. M.; Shima, T.; Wang, L.; Cluff, K. J.; Hampel, F.; Blümel, J.; Gladysz, J. A.; Skopek, K. *J. Am. Chem. Soc.* **2016**, *138*, 7649−7663. (c) Lang, G. M.; Skaper, D.; Hampel, F.; Gladysz, J. A. *Dalton Trans.* **2016**, *45*, 16190−16204. (d) Steigleder, E.; Shima, T.; Lang, G. M.; Ehnbom, A.; Hampel, F.; Gladysz, J. A. *Organometallics* **2017**, *36*, 2891−2901.

(4) (a) Nawara, A. J.; Shima, T.; Hampel, F.; Gladysz, J. A. *J. Am. Chem. Soc.* **2006**, *128*, 4962−4963. (b) Nawara-Hultzsch, A. J.; Stollenz, M.; Barbasiewicz, M.; Szafert, S.; Lis, T.; Hampel, F.; Bhuvanesh, N.; Gladysz, J. A. *Chem. - Eur. J.* **2014**, *20*, 4617−4637.

(5) (a) Wang, L.; Hampel, F.; Gladysz, J. A. *Angew. Chem., Int. Ed.* **2006**, *45*, 4372−4375; *Angew. Chem.* **2006**, *118*, 4479−4482. (b) Wang, L.; Shima, T.; Hampel, F.; Gladysz, J. A. *Chem. Commun.* **2006**, 4075−4077.

DOI: 10.1021/jacs.8b02846
J. Am. Chem. Soc. 2018, 140, 8463−8478

(6) (a) Hess, G. D.; Fiedler, T.; Hampel, F.; Gladysz, J. A. *Inorg. Chem.* **2017**, *56*, 7454−7469. (b) Fiedler, T.; Bhuvanesh, N.; Hampel, F.; Reibenspies, J. H.; Gladysz, J. A. *Dalton Trans.* **2016**, *45*, 7131−7147.
(7) See also (a) Zeits, P. D.; Rachiero, G. P.; Hampel, F.; Reibenspies, J. H.; Gladysz, J. A. *Organometallics* **2012**, *31*, 2854−2877. (b) Lang, G. M.; Bhuvanesh, N.; Reibenspies, J. H.; Gladysz, J. A. *Organometallics* **2016**, *35*, 2873−2889.
(8) (a) Setaka, W.; Yamaguchi, K. *J. Am. Chem. Soc.* **2013**, *135*, 14560−14563 and earlier work cited therein. (b) Setaka, W.; Inoue, K.; Higa, S.; Yoshigai, S.; Kono, H.; Yamaguchi, K. *J. Org. Chem.* **2014**, *79*, 8288−8295. (c) Setaka, W.; Higa, S.; Yamaguchi, K. *Org. Biomol. Chem.* **2014**, *12*, 3354−3357. (d) Shionari, H.; Inagaki, Y.; Yamaguchi, K.; Setaka, W. *Org. Biomol. Chem.* **2015**, *13*, 10511−10516. (e) Nishiyama, Y.; Inagaki, Y.; Yamaguchi, K.; Setaka, W. *J. Org. Chem.* **2015**, *80*, 9959−9966.
(9) In exploratory efforts, the reaction mixture derived from *trans*-**1b** (m = 5) was analyzed by $^{31}P\{^{1}H\}$ NMR. A multitude of signals were present, but chromatography gave a yellowish oil of moderate purity with a $^{31}P\{^{1}H\}$ NMR signal very close to that of *trans*-**2c** (δ/ppm $CDCl_3$: 7.1 vs 7.9, s; $^{1}J_{PPt}$ (satellite) 2393 vs 2398 Hz). The sample decomposed with repeated chromatography.
(10) Kottas, G. S.; Clarke, L. I.; Horinek, D.; Michl, J. *Chem. Rev.* **2005**, *105*, 1281−1376.
(11) For additional relevant platinum complexes, see Taher, D.; Nawara-Hultzsch, A. J.; Bhuvanesh, N.; Hampel, F.; Gladysz, J. A. *J. Organomet. Chem.* **2016**, *821*, 136−141.
(12) (a) Khuong, T.-A. V.; Nuñez, J. E.; Godinez, C. E.; Garcia-Garibay, M. A. *Acc. Chem. Res.* **2006**, *39*, 413−422. (b) Nuñez, J. E.; Natarajan, A.; Khan, S. I.; Garcia-Garibay, M. A. *Org. Lett.* **2007**, *9*, 3559−3561.
(13) (a) Prack, E.; O'Keefe, C. A.; Moore, J. K.; Lai, A.; Lough, A. J.; Macdonald, P. M.; Conradi, M. S.; Schurko, R. W.; Fekl, U. *J. Am. Chem. Soc.* **2015**, *137*, 13464−13467. (b) Li, W.; He, C.-T.; Zeng, Y.; Ji, C.-M.; Du, Z.-Y.; Zhang, W.-X.; Chen, X.-M. *J. Am. Chem. Soc.* **2017**, *139*, 8086−8089.
(14) Nawara-Hultzsch, A. J.; Skopek, K.; Shima, T.; Barbasiewicz, M.; Hess, G. D.; Skaper, D.; Gladysz, J. A. *Z. Naturforsch., B: J. Chem. Sci.* **2010**, *65b*, 414−424.
(15) (a) Marshall, J. A. *Acc. Chem. Res.* **1980**, *13*, 213−218. (b) Chang, M. H.; Dougherty, D. A. *J. Am. Chem. Soc.* **1983**, *105*, 4102−4103. (c) Marshall, J. A.; Audia, V. H.; Jenson, T. M.; Guida, W. C. *Tetrahedron* **1986**, *42*, 1703−1709. (d) Kanomata, N.; Ochiai, Y. *Tetrahedron Lett.* **2001**, *42*, 1045−1048. (e) Ciogli, A.; Dalla Cort, A.; Gasparrini, F.; Lunazzi, L.; Mandolini, L.; Mazzanti, A.; Pasquini, C.; Pierini, M.; Schiaffino, L.; Mihan, F. Y. *J. Org. Chem.* **2008**, *73*, 6108−6118. (f) Castillo, A.; Greer, A. *Struct. Chem.* **2009**, *20*, 399−407. (g) Romuald, C.; Ardá, A.; Clavel, C.; Jiménez-Barbero, J.; Coutrot, F. *Chem. Sci.* **2012**, *3*, 1851−1857.
(16) Estrada, A. L.; Jia, T.; Bhuvanesh, N.; Blümel, J.; Gladysz, J. A. *Eur. J. Inorg. Chem.* **2015**, *2015*, 5318−5321.
(17) Kharel, S.; Joshi, H.; Bierschenk, S.; Stollenz, M.; Taher, D.; Bhuvanesh, N.; Gladysz, J. A. *J. Am. Chem. Soc.* **2017**, *139*, 2172−2175.
(18) (a) Stollenz, M.; Barbasiewicz, M.; Nawara-Hultzsch, A. J.; Fiedler, T.; Laddusaw, R. M.; Bhuvanesh, N.; Gladysz, J. A. *Angew. Chem., Int. Ed.* **2011**, *50*, 6647−6651; *Angew. Chem.* **2011**, *123*, 6777−6781.
(19) Skopek, K.; Barbasiewicz, M.; Hampel, F.; Gladysz, J. A. *Inorg. Chem.* **2008**, *47*, 3474−3476.
(20) Grim, S. O.; Keiter, R. L.; McFarlane, W. *Inorg. Chem.* **1967**, *6*, 1133−1137.
(21) (a) Skopek, K. Doctoral thesis, Universität Erlangen-Nürnberg, 2008. (b) A reviewer has noted that Grubbs' catalyst can contain ruthenium hydride impurities that can effect C═C isomerizations of terminal alkenes. See, for example, Chase, P. A.; Lutz, M.; Spek, A. L.; van Klink, G. P. M.; van Koten, G. *J. Mol. Catal. A: Chem.* **2006**, *254*, 2−19.
(22) Crispini, A.; Harrison, K. N.; Orpen, A. G.; Pringle, P. G.; Wheatcroft, J. R. *J. Chem. Soc., Dalton Trans.* **1996**, 1069−1076.
(23) (a) Ahmad, N.; Ainscough, E. W.; James, T. A.; Robinson, S. D. *J. Chem. Soc., Dalton Trans.* **1973**, 1148−1150. (b) van der Vlugt, J. I.; Ackerstaff, J.; Dijkstra, T. W.; Mills, A. M.; Kooijman, H.; Spek, A. L.; Meetsma, A.; Abbenhuis, H. C. L.; Vogt, D. *Adv. Synth. Catal.* **2004**, *346*, 399−412.
(24) Skopek, K.; Gladysz, J. A. *J. Organomet. Chem.* **2008**, *693*, 857−866.
(25) Another logical product would be the mixed bromide/chloride complex *trans*-$\overline{PtBrCl(P((CH_2)_{14})_3P)}$, and it could be questioned whether this might correspond to the ^{31}P NMR signal assigned to oligomer. In this context, the palladium analog has been characterized[4b] and is easily eluted on a silica gel column. In contrast, the presumedly oligomeric product remains at the origin.
(26) Budzelaar, P. H. M. *gNMR: NMR Simulation Program*, version 5.0.6.0; Adept Scientific: Luton, U.K., 2006.
(27) (a) Boag, N. M.; Kasez, H. D. Technetium and Rhenium. In *Comprehensive Organometallic Chemistry*; Wilkinson, G., Stone, F. G. A., Abel, E. W., Eds; Pergamon: Oxford, 1982; Vol. *4*, pp 173−176. (b) Bauer, E. B.; Hampel, F.; Gladysz, J. A. *Adv. Synth. Catal.* **2004**, *346*, 812−822.
(28) (a) Jung, J. H.; Ono, Y.; Shinkai, S. *Chem. Lett.* **2000**, *29*, 636−637. (b) Aoki, K.; Kudo, M.; Tamaoki, N. *Org. Lett.* **2004**, *6*, 4009−4012. (c) Thalladi, V. R.; Nüsse, M.; Boese, R. *J. Am. Chem. Soc.* **2000**, *122*, 9227−9236.
(29) Alder, R. W.; Butts, C. P.; Orpen, A. G.; Read, D.; Oliva, J. M. *J. Chem. Soc., Perkin Trans. 2* **2001**, 282−287 and references therein.
(30) (a) Bauer, I.; Gruner, M.; Goutal, S.; Habicher, W. D. *Chem. - Eur. J.* **2004**, *10*, 4011−4016. (b) Earlier papers in this series have been reviewed: Bauer, I.; Habicher, W. D. *Collect. Czech. Chem. Commun.* **2004**, *69*, 1195−1230.
(31) (a) Stollenz, M.; Bhuvanesh, N.; Reibenspies, J. H.; Gladysz, J. A. *Organometallics* **2011**, *30*, 6510−6513. (b) Stollenz, M.; Taher, D.; Bhuvanesh, N.; Reibenspies, J. H.; Baranová, Z.; Gladysz, J. A. *Chem. Commun.* **2015**, *51*, 16053−16056.
(32) Lewanzik, N.; Oeser, T.; Blümel, J.; Gladysz, J. A. *J. Mol. Catal. A: Chem.* **2006**, *254*, 20−28.
(33) (a) Bondi, A. *J. Phys. Chem.* **1964**, *68*, 441−451. (b) Mantina, M.; Chamberlin, A. C.; Valero, R.; Cramer, C. J.; Truhlar, D. G. *J. Phys. Chem. A* **2009**, *113*, 5806−5812.
(34) Ehnbom, A. Manuscript in preparation.
(35) (a) Eliel, E. N.; Wilen, S. H. *Stereochemistry of Organic Compounds*; Wiley: New York, 1994; pp 837−838 and 1208. (b) Ward, R. S. *Chemistry in Britain* **1991**, 803−804.
(36) (a) Holt, M. S.; Nelson, J. H. *Inorg. Chem.* **1986**, *25*, 1316−1320. (b) Canac, Y.; Debono, N.; Lepetit, C.; Duhayon, C.; Chauvin, R. *Inorg. Chem.* **2011**, *50*, 10810−10819. (c) Jarvis, A. G.; Sehnal, P. E.; Bajwa, S. E.; Whitwood, A. C.; Zhang, X.; Cheung, M. S.; Lin, Z.; Fairlamb, I. J. S. *Chem. - Eur. J.* **2013**, *19*, 6034−6043.
(37) Cammenga, H. K.; Epple, M. *Angew. Chem., Int. Ed. Engl.* **1995**, *34*, 1171−1187; *Angew. Chem.* **1995**, *107*, 1284−1301. The T_e values best represent the temperature of phase transition or endotherm. DSC measurements were generally not continued above the temperature of initial mass loss (TGA).
(38) This microanalysis poorly or marginally agrees with the empirical formula, but is nonetheless reported as the best obtained to date. The NMR spectra indicate high purities (≥98%). See also Gabbaï, F. P.; Chirik, P. J.; Fogg, D. E.; Meyer, K.; Mindiola, D. J.; Schafer, L. L.; You, S.-L. *Organometallics* **2016**, *35*, 3255−3256.
(39) The $PCH_2CH_2CH_2$ ^{1}H and ^{13}C NMR signals of *cis*-**1g** and *cis*-**2d,g** were assigned by $^{1}H,^{1}H$ COSY, $^{1}H,^{13}C\{^{1}H\}$ COSY, $^{13}C\{^{13}C\}$ COSY, and $^{1}H,^{13}C\{^{1}H\}$ HMBC experiments. Representative spectra have been given for related compounds in earlier papers.[6b,40] The corresponding signals of *cis*-**1f** and *cis*-**2b,c,e,f** were assigned analogously.
(40) Lang, G. M.; Skaper, D.; Shima, T.; Otto, M.; Wang, L.; Gladysz, J. A. *Aust. J. Chem.* **2015**, *68*, 1342−1351.
(41) The J values given for virtual triplets represent the *apparent* couplings between adjacent peaks and not the mathematically rigorous coupling constants. See Hersh, W. H. *J. Chem. Educ.* **1997**, *74*, 1485−1488.
(42) This coupling represents a satellite (d, ^{195}Pt = 33.8%) and is not reflected in the peak multiplicity given.

DOI: 10.1021/jacs.8b02846
J. Am. Chem. Soc. 2018, 140, 8463−8478

(43) FAB, 3-NBA, *m*/*z* (relative intensity, %); the most intense peak of the isotope envelope is given.
(44) The *ortho* proton signal was assigned by analogy to that of *trans*-**6c** (two downfield signals due to restricted Pt−C_{ipso} rotation, δ 7.38 and 7.08, 2d, $^3J_{HH}$ = 7.0−7.2 Hz).[4b] The chemical shifts and multiplicities of the *meta* and *para* proton signals are also in close agreement.
(45) The signal for the *ipso* phenyl carbon atom was not observed.
(46) Schmidt, S. P.; Trogler, W. C.; Basolo, F.; Urbancic, M. A.; Shapley, J. R. *Inorg. Synth.* **1985**, *23*, 41−46.
(47) The P$CH_2CH_2CH_2$ ^{1}H and ^{13}C NMR signals of *fac*-**10c** were assigned by ^{1}H,^{1}H COSY and ^{1}H,^{13}C{^{1}H} COSY experiments. The corresponding signals of *fac*-**11c**, *fac*-**12′c**, and *fac*-**13′c** were assigned analogously.
(48) The exact mass of the most intense $[M]^+$ peak should be 1034.56. It is presumed that the instrument, which provides masses to the nearest whole integer, rounded the value down, and thus it does not represent the ion $[M - H]^+$. All peak assignments were checked versus the theoretical isotope envelope pattern.
(49) The situation with this ion is similar to that described in ref 48.
(50) These dirhenium peaks deviate by as many as ±3 mass units from that expected for the ion given. However, the isotope envelopes are otherwise in good agreement with those calculated.
(51) The situation with this ion is similar to that described in ref 48 (calculated exact mass of most intense $[M]^+$ peak = 994.42; the instrument is presumed to have rounded the value up, such that it does not represent the ion $[M + H]^+$).
(52) The situation with this ion is similar to that described in ref 51.
(53) One peak of this triplet is obscured; the chemical shift and coupling constant are extrapolated from the two that are visible.
(54) This reaction was carried out with a Fischer−Porter bottle and H_2 (5 bar), instead of a balloon pressure of H_2 (1 bar).
(55) Macrae, C. F.; Bruno, I. J.; Chisholm, J. A.; Edgington, P. R.; McCabe, P.; Pidcock, E.; Rodriguez-Monge, L.; Taylor, R.; van de Streek, J.; Wood, P. A. *J. Appl. Crystallogr.* **2008**, *41*, 466−470.
(56) Lichtenberger, D. L.; Gladysz, J. A. *Organometallics* **2014**, *33*, 835−835.

DOI: 10.1021/jacs.8b02846
J. Am. Chem. Soc. 2018, 140, 8463−8478